Online supplemental data

Effects of noise on vascular function oxidative stress and inflammation – mechanistic insight from studies in mice

Thomas Münzel MD[1,2], Andreas Daiber[1,2], Sebastian Steven[1], Lan P. Tran[1], Elisabeth Ullmann[1], Sabine Kossmann[1], Frank P. Schmidt[1], Matthias Oelze[1], Ning Xia[3], Huige Li[3], Antonio Pinto[4], Philipp Wild[2,4], Kai Pies[5], Erwin R. Schmidt[6], Steffen Rapp[6], Swenja Kröller-Schön[1]

From the [1] Center for Cardiology, Cardiology I – Laboratory of Molecular Cardiology, [2] German Center for Cardiovascular Research (DZHK), Partner Site Rhine-Main, [3] Department of Pharmacology, [4] Preventive Cardiology and Preventive Medicine, Center for Cardiology; University Medical Center of the Johannes Gutenberg-University Mainz, Mainz, Germany, [5] Engineer for Noise Protection, Mainz, Germany, [6] Institute for Molecular Genetics, Johannes Gutenberg University, Mainz, Germany.

Supplemental Material and Methods

Animals

All animals were treated in accordance with the Guide for the Care and Use of Laboratory Animals as adopted by the U.S. National Institutes of Health and approval was granted by the Ethics Committee of the University Hospital Mainz and the Landesuntersuchungsamt Rheinland-Pfalz (Koblenz, Germany; permit number: 23 177-07/G 12-1-021 E3 and 23 177-07/G 15-1-094). After the indicated duration of noise exposure (see below), animals were killed under isoflurane anesthesia by transection of the diaphragm and removal of the heart and thoracic aorta. Glucose levels were assessed in whole blood using the ACCU-CHEK Sensor system from Roche Diagnostics GmbH (Mannheim, Germany).

Isometric tension studies

Perivascular fat was removed from every aorta, which were then cut into 4-mm segments. Rings were mounted on force transducers in organ bad chambers, pre-constricted with prostaglandin $F_{2\alpha}$ (yielding approximately 80 % of the maximal tone induced by KCl bolus) and concentration-relaxation curves in response to increasing concentrations of acetylcholine (ACh) and nitroglycerin (GTN) were performed as described [1, 2]. Sensitivity to vasoconstrictors norepinephrine and endothelin-1 was tested by exposure of aortic ring segments to cumulative concentrations of the vasoconstrictors as described [19, 20].

Detection of serum cholesterol, triglyceride, HDL and glucose

Serum cholesterol, triglyceride, high-density lipoprotein (HDL) and glucose levels were analyzed in the Department of Clinical Chemistry, University Hospital Mainz, Germany, using the daily routine facilities for in-patient care.

ELISA for catecholamines and angiotensin-II

Circulating catecholamines (dopamine, adrenalin, noradrenalin) were determined in mouse serum using a commercial enzyme-linked immunosorbent assay (ELISA) kit (TriCat, IBL, Hamburg, Germany) following the instructions of the vendor [3]. Serum angiotensin-II levels were measured using a commercial enzyme-linked immunosorbent assay (ELISA) kit (RAB0010, SIGMA Aldrich) following the instructions of the vendor. Cortisol urine and kidney levels were determined by

commercial ELISA (in urine: # RE52241; in kidney: # RE52061, IBL International GmbH, Hamburg, Germany).

Histological and immunohistochemical staining of aortic rings

Paraffin-embedded aortic samples were stained with primary antibodies against 3-nitrotyrosine (3NT) (1:200, Merck-Millipore, Darmstadt, Germany) [4]. ET-1 staining was performed using specific antibodies (Pierce #MA3-005: 1:200; Abcam #117757: 1:450). 4-hydroxynonenal (4HNE) staining was conducted using a specific antibody (mouse monoclonal, 1:100 dilution, Percipio Biosciences #24325). Depending upon the species of primary antibodies, appropriate biotinylated (anti-mouse: Vector Lab., Burlingame, CA; anti-rabbit: Thermo Fisher Scientific, Waltham, MA) secondary antibodies were used at dilutions according to the manufacturer's instructions. For immunochemical detection ABC reagent (Vector) and then DAB reagent (peroxidase substrate Kit, Vector) were used as substrates. Quantification was performed using Image ProPlus 7.0 software (Media Cybernetics, Rockville, MD).

Detection of oxidative stress and inflammation in plasma, cardiac tissue and aorta

Vascular ROS formation was determined using dihydroethidium (DHE, 1 µM)-dependent fluorescence microtopography in aortic cryo-sections as described [5, 6]. To investigate the involvement of eNOS uncoupling in ROS production and endothelial dysfunction, aortic rings were preincubated with the NOS inhibitor L-NAME (0.5 mM) [5-7]. ROS-derived red fluorescence was detected using a Zeiss Axiovert 40 CFL microscope, Zeiss lenses and Axiocam MRm camera. Superoxide formation in heart membrane fractions was measured by lucigenin (5 µM) ECL in the presence of NADPH (200 µM) as previously described [6]. Protein tyrosine nitration was detected using a specific antibody for 3-nitrotyrosine (3NT, 1:1,000, Upstate Biotechnology, MA, USA) and lipid peroxidation using a specific antibody for malondialdehyde (MDA)-positive proteins (1:1,000, Calbiochem, Darmstadt, Germany) in EDTA plasma. Inflammation was detected using a specific antibody for interleukin-6 (anti IL-6 rabbit antibody, abcam, ab6672) in EDTA plasma. Briefly, 100 µl (0.5 µg/µl protein based on Bradford analysis) of the EDTA plasma were transferred to a Protran BA85 (0.45 µm) nitrocellulose membrane (Schleicher&Schuell, Dassel, Germany) by a

Minifold I vacuum Dot-Blot system (Schleicher&Schuell, Dassel, Germany). Each slot was washed twice with 200 µl PBS before and after protein transfer. The membrane was dried for 60 min at 60 °C. With a similar procedure 3-nitrotyrosine-positive proteins were measured in cardiac tissue homogenates (30 µg cardiac protein based on Bradford assay per well). Positive bands were detected by enhanced chemiluminescence after incubation with a peroxidase-coupled secondary antibody (GAM-POX and GAR-POX, 1:10,000) (Vector Laboratories, CA, USA). All incubation and washing steps were performed according to the manufacturer's instructions. Densitometric quantification of the dots was performed using the Super Signal ECL kit from Thermo Scientific.

S-glutathionylation of endothelial nitric oxide synthase by immunoprecipitation

Immunoprecipitation of eNOS and subsequent immunoblotting of the precipitate for S-glutathionylation was performed according to a standard protocol as recently published [8]. M-280 sheep anti-mouse IgG coated beads from Invitrogen (Darmstadt, Germany) were used along with a monoclonal mouse eNOS (Biosciences, USA) antibody. The beads were loaded with the eNOS antibody and cross-linked according to the manufacturer's instructions. Next, cardiac and aortic homogenates were incubated with the eNOS antibody beads, precipitated with a magnet, washed and transferred to the gel and subjected to SDS-PAGE followed by a standard Western blot procedure using a monoclonal mouse antibody against S-glutathionylated proteins from Virogen (Watertown, MA, USA) at a dilution of 1:1,000 under non-reducing conditions. After stripping of the membrane, the bands were immunoblotted for eNOS (mouse monoclonal, 1:1,000, BD Biosciences, USA) to allow normalization of the signals. Detection and quantification were performed by enhanced chemiluminescence (ECL) with peroxidase conjugated anti–mouse (1:10,000, Vector Lab., Burlingame, CA) secondary antibodies. Densitometric quantification of antibody-specific bands was performed with a ChemiLux Imager (CsX-1400M, Intas, Göttingen, Germany) and Gel-Pro Analyzer software (Media Cybernetics, Bethesda, MD).

Western Blotting Analysis of Other Proteins

The procedures were similar to those described above but aortic or heart tissue and lung endothelial cells (MLEC) were used in all Western blot experiments.

Protein samples were analyzed by Western blot analysis for endothelial NO-synthase (eNOS, mouse monoclonal, 1:1000, BD Biosciences, USA), phospho-Ser1177-eNOS (rabbit polyclonal, 1:1000, Cell Signaling, Danvers, MA, USA), dihydrofolate reductase (DHFR, mouse monoclonal, 1 µg/ml, Abnova Corp., Germany), GTP-cyclohydrolase-1 (GCH-1, mouse monoclonal, 1 µg/ml, Abnova Corp., Germany), $sGC\alpha_1$ and $sGC\beta_1$ (rabbit polyclonal, 1:10000 and 1:500, Abcam, Cambridge, UK), phospho-Ser239-VASP (mouse monoclonal, 1.5µg/ml, Millipore, Billierica, MA, USA), cGMP-dependent protein kinase (cGK-1, goat polyclonal, 1:200, SantaCruz, Dallas, USA) NADPH oxidase isoform 1 and 2 (Nox1, rabbit polyclonal, 1:500, Abcam, Cambridge, MA, USA and Nox2 ($gp91^{phox}$), mouse monoclonal, 1:1,000, BD Biosciences, USA), endothelin-1 (ET-1, rabbit polyclonal, 1:5000, Abcam, Cambridge, MA, USA) and monoclonal mouse α-actinin or polyclonal rabbit β-actin (both 1:2500, Sigma-Aldrich) for normalization of loading and transfer. Secondary antibodies (GAM-POX, GAR-POX, donkey anti goat-peroxidase labeled, 1:5000, Santa Cruz, USA) and ECL development as described above for dot blot.

Quantitative reverse transcription real-time PCR (qRT-PCR)

Total mRNA from MLECs and aortic tissue was isolated using the RNeasy Fibrous Tissue Mini Kit, Qiagen, Hilden, Germany according to the manufacturers protocol. 50 ng of total RNA was used for quantitative reverse transcription real-time PCR (qRT-PCR) analysis using QuantiTect Probe RT-PCR kit (Qiagen) as described previously. [21, 29] Primer-Probe-Mixes purchased from Applied Biosystems, Foster City, CA were used to analyse the mRNA expression patterns of endothelial NO Synthase (eNOS, Mm_00435204_m1), heme oxygenase-1 (HO-1, Mm_00516004_m1), NADPH oxidase -1 (NOX-1, Mm_00549170_m1) and PPARγ transcription co-factor-1α (PGC-1α, Mm_01208835_m1) normalized on the TATA box binding protein (TBP, Mm_00446973_m1) as an internal control. For quantification of the relative mRNA expression the comparative ΔΔCt method was used. Gene expression of target gene in each sample was expressed as the percentage of wildtype.

Aortic nitric oxide formation by electron spin resonance (EPR) spectroscopy

Aortic nitric oxide formation was measured using EPR-based spin trapping with iron-diethyldithiocarbamate ($Fe(DETC)_2$) colloid which was freshly prepared

under argon as described [9]. One murine aorta was cut into ring segments of 3 mm length (6-7 pieces) and placed in 1 ml Krebs-Hepes buffer on a 24-well plate on ice. The samples were stimulated with 10 µM calcium ionophore (A23187) for 2 min on ice, then 1 ml of the $Fe(DETC)_2$ colloid solution (400 µM in PBS with Ca^{2+}/Mg^{2+}) was added and the plate was placed in the incubator at 37 °C. After 60 min of incubation, the aortic rings were placed at a fixed position in a 1 ml syringe with removed top in PBS buffer and frozen in liquid nitrogen (in the way that the entire aortic sample was placed within a 100 µl volume of the syringe). For measurement, the frozen cylinder with the aortic sample was pressed out of the syringe and placed in a special Dewar vessel (Magnettech, Berlin, Germany) filled with liquid nitrogen. The localization of the aortic sample was adjusted to the middle of the resonator. EPR conditions: B_0= 3276 G, sweep=115 G, sweep time=60 s, modulation=7000 mG, MW power=10 mW, gain=$9x10^2$ using a Miniscope MS400 from Magnettech (Berlin, Germany). As previously reported, the A23187-stimulated NO signal was absent when the aortas were denuded, L-NAME (200 µM) was added or when aorta from $eNOS^{-/-}$ mice were used (not shown). The general conditions for this assay were previously described by Kleschyov et al. [10].

Isolation of mouse lung endothelial cells (MLEC)

Mouse lung endothelial cells were isolated using collagenase I for digestion of freshly isolated mouse lungs. Two separation steps were performed to separate endothelial cells from the others using CD31 MACS beads (Miltenyi Biotech, Bergisch Gladbach, Germany) and ICAM dynabeads (Thermo fisher, Dreieich, Germany) according to the manufacturer's protocols.

Non-invasive blood pressure measurements (NIBP)

NIBP measurements were performed on a daily basis throughout the noise exposure regimen (CODA 2, Kent Scientific, Torrington, USA). Animals were placed in restraining tubes on a preheated plate (32°C). The CODA System relies on two tail-cuffs to measure blood pressure. An occlusion cuff and a volume-pressure recording cuff are positioned on the tail. Data have been acquired by CODA data Acquisition Software. Five measurements were performed in advance to get the animal used to it. The mean values of ten NIBP readings were used for each animal.

Feng et al. proofed accuracy of this method compared to radiotelemetric measurement [11].

FACS analysis of the aorta

Flow cytometry of aortas was performed like described previously [12, 13]. Briefly, aortic vessels were cleaned of fatty tissue, minced and digested with liberase™ (1 mg/ml, Roche, Basel, Switzerland) for 30 min at 37°C. By passing the lysed aortic fragments through a cell strainer (70 µm), a single-cell suspension was obtained. Single-cell suspensions were treated with Fc-block (anti-CD16/CD32), washed and surface-stained with CD45 APC-efluor 780 (30-F11), TCR-β V450 (H57-597, BD Biosciences, San Jose, CA, NK1.1 PE-Cy7 (Pk136), CD11b PE (M1/70, BD Biosciences, San Jose, CA), Ly6G FITC (1A8, BD Biosciences, San Jose, CA), F4/80 APC (BM8), Ly6C PerCP-Cy.5.5 (AL-21) (all antibodies from eBioscience (San Diego, CA) unless stated otherwise). Dead cells were excluded by staining with Fixable Viability Dye eFluor506 (eBioscience, San Diego, CA). Based on a live gate, events were acquired and analyzed using a BD FACS CANTO II flow cytometer (Becton Dickinson, Franklin Lakes, NJ) and FACSDiva software (Becton Dickinson, Franklin Lakes, NJ), respectively.

Next generation sequencing

RNA extraction

The tissue samples (aorta) used for RNA extraction were carefully excised and immediately frozen in liquid nitrogen. For the initial Illumina RNA-Seq, tissue samples from four animals were pooled und subjected to total RNA isolation. For replicate datasets, four tissues samples of control and noise treated mice were extracted in parallel. Total RNA was isolated using the RNA extraction kit (PEQLab precellys™, VWR, Darmstadt, Germany) following the manufacturer's instructions. RNA concentration and integrity were assessed with a Bioanalyzer 2100 (Agilent RNA Nano or Pico chips Agilent Technologies, Santa Clara, USA).

Illumina sequencing

For RNA-Seq library construction 0.5 – 1.0 µg of total RNA of each tissue sample were used. The RNA quality as assessed by the RNA Integrity Number (RIN) values were between 6 and 8. Sequencing libraries were constructed using the library preparation kit TruSeq Stranded mRNA™ according to the instructions by the

manufacturer (Illumina, San Diego, USA). The sequencing of the cDNA sequencing libraries was carried out as 150 bp paired-end runs on an Illumina NexSeq500^{TM} (Illumina, San Diego, USA) by StarSEQ GmbH Mainz, Germany. The raw RNA-seq data was processed with house internal perl scripts to do quality trimming to a Phred score of > 30, remove sequencing adapters and primers. The summary of sequencing statistic is given in suppl. Table 1S.

Analysis of Illumina RNA-Seq data

Paired end reads were mapped against UCSC mouse genome build GRCm38/mm10 (Dec. 2011) using STAR [14] combined with the RSEM [15] data analyzing pipeline with the default settings. Results were processed in R [16] (Version 3.3.1) using DESeq2 [17] package for calling differential gene expression. Principal component analysis and calculation of Cook's distances were performed using DESeq2. In general, a gene was considered as differentially expressed if the adjusted p-value was < 0.05. For the analysis and visualization of gene expression changes in pathway systems gene symbols were converted to Entrez/KEGG gene ids and log2 fold changes of gene subsets were extracted. Gene sets were mapped to selected KEGG [18, 19] pathways using Pathview [20] package. Mappings and generation of pathway figures were done with default settings.

Differential expression of single genes and small subsets of genes were analyzed based on FPKM values of the RSEM results. Expression values were extracted without consideration of DESeq2 generated p-values. Significance of expression changes compared to the untreated controls was checked by one-way ANOVA with Bonferroni's correction (Prism for Windows, version 7.01, GraphPad Software Inc.). The promoters of the eight most regulated genes were analysed for HMR conserved transcription factor binding sites on the basis of the Transfac database.

Materials

For isometric tension studies, nitroglycerin (GTN) was used from a Nitrolingual infusion solution (1 mg/ml) from G.Pohl-Boskamp (Hohenlockstedt, Germany). L-012 (8-amino-5-chloro-7-phenylpyrido[3,4-d]pyridazine-1,4-(2H,3H)dione sodium salt) was purchased from Wako Pure Chemical Industries (Osaka, Japan). Endothelin-1 was obtained from Bachem AG (Bubendorf, Switzerland). The QuantiTect probe RT-PCR Kit was purchased from Qiagen (Hilden, Germany) and TaqMan probes from

Applied Biosystems (Darmstadt, Germany). The Bradford reagent was obtained from BioRad, Munich, Germany. All other chemicals were of analytical grade and were obtained from Sigma-Aldrich, Fluka or Merck.

Statistical analysis

Results are expressed as the means ± SD. Two-way ANOVA (with Bonferroni's correction for comparison of multiple means) was used for comparisons of concentration-relaxation curves (Prism for Windows, version 6.05, GraphPad Software Inc.). One-way ANOVA (with Bonferroni's correction for comparison of multiple means) or, where appropriate, equivalent non-parametric test (Dunn / Kruskal-Wallis multiple comparison) was used for comparisons of weight gain, blood glucose, other serum/plasma parameters, such as triglycerides, 3-nitrotyrosine, MDA, histological data, aortic ROS formation, protein and mRNA expression, cardiac and whole blood oxidative stress, aortic NO formation, blood pressure (SigmaStat for Windows, version 3.5, Systat Software Inc.). p-values < 0.05 were considered as statistically significant and are either provided in the figures or by symbol legends of tables. The number of replicates in the different assays may vary since not all animals were used in all assays.

Statistical sample size calculation

An a priori power analysis was performed to estimate the numbers of mice needed for significant results. Differences in flow mediated dilation measured in an human aircraft noise study were used as calculation basis [21]. Following input parameters were used for the computation of sample size effect size = 0.8, alpha = 0.05, Power (1-beta) = 0.95. The analysis was performed for an one tailed parametric test between two groups with independent means with the freely available G*Power Software [22]. An overall sample size of n = 70 (with Df = 68) with equal group allocation was calculated. All animal experiments planning were guided by this initial sample size estimation, which helped preventing unnecessary test animal breeding and loss.

[40] *-- Thursday, December 08, 2016 -- 18:02:01*

t tests - Means: Difference between two independent means (two groups)

Analysis: A priori: Compute required sample size

Input:	Tail(s)	=	One
	Effect size d	=	0.8
	α err prob	=	0.05
	Power (1-β err prob)	=	0.95
	Allocation ratio N2/N1	=	1
Output:	Noncentrality parameter δ	=	3.3466401
	Critical t	=	1.6675723
	Df	=	68
	Sample size group 1	=	35
	Sample size group 2	=	35
	Total sample size	=	70
	Actual power	=	0.9523628

Supplemental Discussion

Next generation sequencing

Zbtb44 codes for a highly conserved zinc finger domain DNA binding protein. It is involved in stem cell growth and responds to steroid and adrenergic stimulation [23, 24]. The specific function in the cardiovascular vessels has not been determined. SERTAD4 is highly expressed in adult murine fibrous tissues. SERTAD4 resides predominantly in the nucleus throughout cell cycle progression and shows interaction with PP2A and PI3K [25, 26], which are crucial regulators in the here displayed pathways. Yipee-like 2 (YPEL2) is localized in the nucleus and contains several metal binding sites, it is known to interact with phosphatases and influences calcium signalling in cellular repolarisation [27]. Indian Hedgehog (IHH) is involved in signalling and has been found among other pathways to participate in cartilage degeneration as well as in TGFbeta-driven chondrogenesis and ossification [28, 29]. Sacsin is highly expressed in the central nervous tissue but shows also abundant expression in fibrous tissue. It has chaperone like function and is regulated by TGFbeta in epithelial mesenchymal transition [30]. Nbeal1 is known to be strongly expressed in mouse aorta, its lysosomal import sequence may implicate a role in autophagy and hypoxia [31]. PTPN4 belongs to a superfamily of protein phosphatases, which is associated with cytoskeletal proteins. It has a role in cell growth and motility in various tissues and cell lines [32]. Downregulation of the nuclear orphan receptor NR4A3/NOR1 is known to contribute to the regulation of matrix metallo-protease in vascular tissue and to the activation of VSMC [33, 34]. Conservative promoter database analysis of transcription factor binding sites of the corresponding gene products showed many binding sites with redox-active and cysteine rich transcription factors (NFkB, Foxo and zinc-finger proteins) in the promoter regions of the 8 most regulated genes (not shown). This might insinuate that noise generated nitro-oxidative stress may directly influence transcription levels. Although these genes and their gene products are not well known in the cardiovascular context, through their interaction partners they strongly contribute to the here depicted pathways.

In the setting of stress-induced vasoconstriction the TGFbeta pathway and the smooth muscle pathway are highly relevant (suppl. Figure 12S). The patterns in the smooth muscle pathway indicate a change in contractility and reduced actin expression. Changed actin expression may be indicative for myofibroblast formation which is an early step in vascular remodelling [35]. Similarly by decreased endogenous

TGFbeta expression the differentiation to myofibroblasts and osteoblasts by Smad signalling is enforced and may lead to extracellular matrix remodelling and increased arterial stiffness. Those assumptions are supported by the evaluation of apoptosis, cell cycle, NFκB pathways and integrin levels in focal adhesion, as they demonstrate by their significant regulation that the aortic tissue has left the quiescent status and is undergoing proliferative and morphologic changes. Kinase activity and Foxo transcription factor regulation further corroborates this conclusion (suppl. Figures 13S and 14S).

The results of changes in the adrenergic signaling pathway support the ELISA results and the non-invasive blood pressure measurements (suppl. Figure 13S). Quality measures of NGS sampling like total number of reads and reads after trimming (suppl. Table S1) and overall expression variance (suppl. Figures 15S A) did not show any major discrepancies between samples. However PCA analysis revealed that two Day 2 samples strongly deviated from all other samples (suppl. Figure 15S B). Therefore we decided to generate an alternative analysis of the VSMC pathway without those samples, giving only slightly divergent results (suppl. Figure 16S).

Supplemental Table 1S. *Sequencing Statistics*

		Total Number of Reads	Reads after Trimming	% of trimmed Reads
Sample_B6_Pool1		53,197,578	50,025,387	-5.96%
Sample_B6_Pool2	WT	44,177,732	41,420,817	-6.24%
Sample_B6_Pool3	untreated	63,680,912	59,647,937	-6.33%
Sample_B6_Pool4		95,096,196	89,464,809	-5.92%
Sample_5		37,674,372	35,632,459	-5.42%
Sample_6	+noise	75,294,996	70,702,144	-6.10%
Sample_7	(1 day)	46,201,474	43,604,821	-5.62%
Sample_8		35,506,696	33,188,259	-6.53%
Sample_9		46,348,626	43,476,457	-6.20%
Sample_10	+noise	67,370,490	63,227,108	-6.15%
Sample_11	(2 days)	72,033,100	67,470,353	-6.33%
Sample_12		63,030,112	59,139,369	-6.17%
Sample_13		33,610,426	31,440,416	-6.46%
Sample_14	+noise	90,003,020	84,704,210	-5.89%
Sample_15	(4 days)	72,226,828	67,936,404	-5.94%
Sample_16		108,203,920	101,792,381	-5.93%

For gene expression profiling of mouse aorta tissue after noise exposure a total of 16 sample pools of four conditions were sequenced on Illumina NextSeq 500. For each pool between 33,361,426 and 108,203,920 high quality 150 nt „paired end“ reads were generated.

Table 2S. *Effects of noise exposure on Potency (pD_2) and Maximal Relaxation (Max. Relax.) to ACh and GTN*

	ACh		GTN	
	pD_2 (-log[ED_{50}])	**Max. Rel. %**	**pD_2 (-log[ED_{50}])**	**Max. Rel. %**
Ctr	-7.15 ±0.24	81.4 ±7.8	-6.95 ±0.28	87.3 ±8.1
+noise (1 day)	-7.04 ±0.31*	67.8 ±14.6*	-6.82 ±0.19*	75.2 ±9.8*
+noise (2 days)	-7.03 ±0.31*	69.0 ±9.8*	-6.64 ±0.50*	83.0 ±6.4*#
+noise (4 days)	-7.07 ±0.25	63.4 ±10.6*	-6.91 ±0.31§	85.0 ±11.1#

Data are mean ± SD from 13-26 mice/group. P<0.05: *vs. Ctr (no noise) , #vs. +noise (1 day) ; §vs. +noise (2 days)

Table 3S. *Effects of noise exposure on Potency (pD_2) and Maximal Constriction (Max. Constr.) to Norepinephrine (NE) and ET-1*

	NE		***ET-1***	
	pD_2 (-log[ED_{50}])	**Max. Constr. %**	**pD_2 (-log[ED_{50}])**	**Max. Constr. %**
Ctr	-7.48 ±0.21	46.5 ±17.5	-7.17 ±0.72	24.0 ±21.5
+noise (1 day)	-7.51 ±0.18	55.4 ±26.6	-7.03 ±0.74	41.1 ±29.4*
+noise (2 days)	-7.44 ±0.13	58.5 ±20.2*	-7.16 ±0.64	38.5 ±20.3*
+noise (4 days)	-7.48 ±0.15	68.9 ±25.5*	-7.39 ±0.62#	31.0 ±25.9

Data are mean ± SD from 8-22 mice/group. P<0.05: *vs. Ctr (no noise)

Supplemental Table 4S. *30 most highly upregulated genes over all three treated conditions*

		Log2FoldChange			***Description***
Gene ID	**Gene Symbol**	+ noise (1 day)	+ noise (2 days)	+ noise (4 days)	
29884	*Zbtb44*	0.75	0.72	0.97	zinc finger and BTB domain containing 44
1655	*Sertad4*	0.67	0.74	0.86	SERTA domain containing 4
515	*Ihh*	0.71	0.66	0.85	Indian hedgehog homolog
4699	*Ypel2*	0.59	0.72	0.88	yippee-like 2
30225	*AK011526*	0.73	0.56	0.74	chr9:50745720-50746509 (GRCm38/mm10)
30572	*Smad6*	0.72	0.65	0.58	SMAD family member 6
28098	*Prr33*	0.72	0.60	0.61	proline rich 33
18272	*Larp1b*	0.68	0.52	0.64	La ribonucleoprotein domain family, member 1B
24429	*Grip2*	0.65	0.53	0.65	glutamate receptor interacting protein 2
21072	*Tmem82*	0.71	0.46	0.65	transmembrane protein 82
21279	*AK083203*	0.63	0.48	0.61	chr4:154637576-154644716 (GRCm38/mm10)
18333	*Smad9*	0.58	0.56	0.57	SMAD family member 9
19025	*AK039581*	0.57	0.49	0.60	chr3:107440341-107442976 (GRCm38/mm10)
18673	*S100a7a*	0.70	0.43	0.53	S100 calcium binding protein A7A
6670	*Xrcc3*	0.56	0.43	0.62	X-ray repair complementing defective repair in Chinese hamster cells 3
5065	*Aoc2*	0.57	0.55	0.48	similar to Membrane copper amine oxidase (Vascular adhesion protein-1) (VAP-1) (HPAO)
29793	*Pde4a*	0.62	0.48	0.48	phosphodiesterase 4A, cAMP specific
16324	*Lrp4*	0.48	0.60	0.48	low density lipoprotein receptor-related protein 4
4040	*2810021J22Rik*	0.50	0.49	0.57	similar to KRAB-zinc finger protein 68
14878	*AI606181*	0.48	0.45	0.59	chr19:41593363-41594110 (GRCm38/mm10)
16882	*Pla2g4b*	0.61	0.49	0.42	Phospholipase A2 Group IVB
21073	*AI507597*	0.48	0.42	0.61	long non-coding RNA
27927	*AK084972*	0.55	0.41	0.55	
14591	*Dtx4*	0.45	0.45	0.60	deltex 4 homolog (Drosophila)
13036	*Gm20219*	0.56	0.41	0.53	predicted gene
2482	*Arid3a*	0.38	0.50	0.62	AT rich interactive domain 3A (Bright like)
3800	*Adam19*	0.52	0.49	0.48	ADAM metallopeptidase domain 19 (meltrin beta)
21278	*5930403L14Rik*	0.50	0.45	0.52	RIKEN cDNA 5930403L14 gene
21876	*Fam184b*	0.41	0.49	0.57	family with sequence similarity 184, member B
1016	*Pik3c2b*	0.49	0.48	0.51	phosphoinositide-3-kinase, class 2, beta polypeptide

Expression profiling (DESeq2) investigating aorta tissue showed 983 at least significant differentially expressed genes ($p < 0.05$) in one treated group. 532 of these genes are higher expressed after noise treatment compared to untreated controls. The 30 most upregulated genes are shown with expression changes of all three conditions compared to untreated controls.

Supplemental Table 5S. *30 most highly downregulated genes over all three treated conditions*

		Log2FoldChange			Description
Gene ID	**Gene Symbol**	+ noise (1 day)	+ noise (2 days)	+ noise (4 days)	
9043	*Sacs*	-1.66	-1.59	-1.83	Sacsin, spastic ataxia of Charlevoix-Saguenay
393	*Nbeal1*	-1.50	-1.37	-1.55	neurobeachin like 1
906	*Ptpn4*	-1.25	-1.06	-1.19	protein tyrosine phosphatase, non-receptor type 4
19865	*Nr4a3*	-1.15	-0.99	-1.22	nuclear receptor subfamily 4, group A, member 3
5907	*Klhl28*	-1.08	-0.85	-1.07	kelch-like 28 (Drosophila)
6749	*Itgb8*	-1.06	-0.93	-1.04	integrin, beta 8
32555	*Tsc22d3*	-1.03	-1.08	-1.33	TSC22 domain family, member 3
19145	*Myoz2*	-0.99	-0.78	-0.72	myozenin 2
3638	*Peli1*	-0.94	-0.80	-1.03	Pellino E3 Ubiquitin Protein Ligase 1
26440	*Ube3a*	-0.91	-0.72	-0.95	similar to ubiquitin protein ligase E3A
21142	*Gm13212*	-0.90	-0.77	-0.83	predicted gene 13212; Chr4:145585166-145625345 bp, + strand
22300	*BC005561*	-0.90	-0.85	-1.10	THO complex 2; cDNA sequence BC005561
9468	*Lmbrd2*	-0.88	-0.77	-0.91	LMBR1 domain containing 2
23482	*C1galt1*	-0.87	-0.74	-1.06	core 1 synthase, glycoprotein-N-acetylgalactosamine 3-beta-galactosyltransferase, 1
32389	*Brwd3*	-0.86	-0.68	-0.80	bromodomain and WD repeat domain containing 3
17104	*AK154258*	-0.86	-1.05	-1.02	chr2:132559005-132561681 (GRCm38/mm10)
5848	*Arhgap5*	-0.86	-0.69	-0.82	Rho GTPase activating protein 5
11434	*Adamts1*	-0.85	-0.47	-1.08	a disintegrin-like and metallopeptidase (reprolysin type) with thrombospondin type 1 motif, 1
8104	*Fam107a*	-0.84	-1.06	-1.11	family with sequence similarity 107, member A
19433	*Trp53inp1*	-0.82	-0.79	-0.97	transformation related protein 53 inducible nuclear protein 1
11760	*AK137492*	-0.81	-0.73	-0.93	hypothetical Annexin/TONB Box N terminus containing protein
29111	*Mt2*	-0.78	-0.67	-0.83	metallothionein 2, methyltransferase 2
6797	*Actn2*	-0.78	-0.76	-0.86	actinin, alpha 2
7813	*Homer1*	-0.76	-0.70	-0.88	homer homolog 1
20885	*Fam46b*	-0.75	-1.17	-1.13	family with sequence similarity 46, member B
14873	*Lcor*	-0.73	-0.67	-0.87	ligand dependent nuclear receptor corepressor
9257	*Dgkh*	-0.72	-0.75	-0.97	diacylglycerol kinase, eta
4229	*Per1*	-0.62	-0.75	-1.28	period homolog 1, 1-Cys-peroxiredoxine
7661	*BC057675*	-0.60	-0.70	-0.97	chr13:68216278-68236984 (GRCm38/mm10)
24411	*Klf15*	-0.55	-0.91	-1.07	Krueppel-like factor 15

The Table shows the 30 most downregulated of 451 genes, which were lower expressed in aorta of noise treated mice then in the untreated controls. ($p < 0.05$).

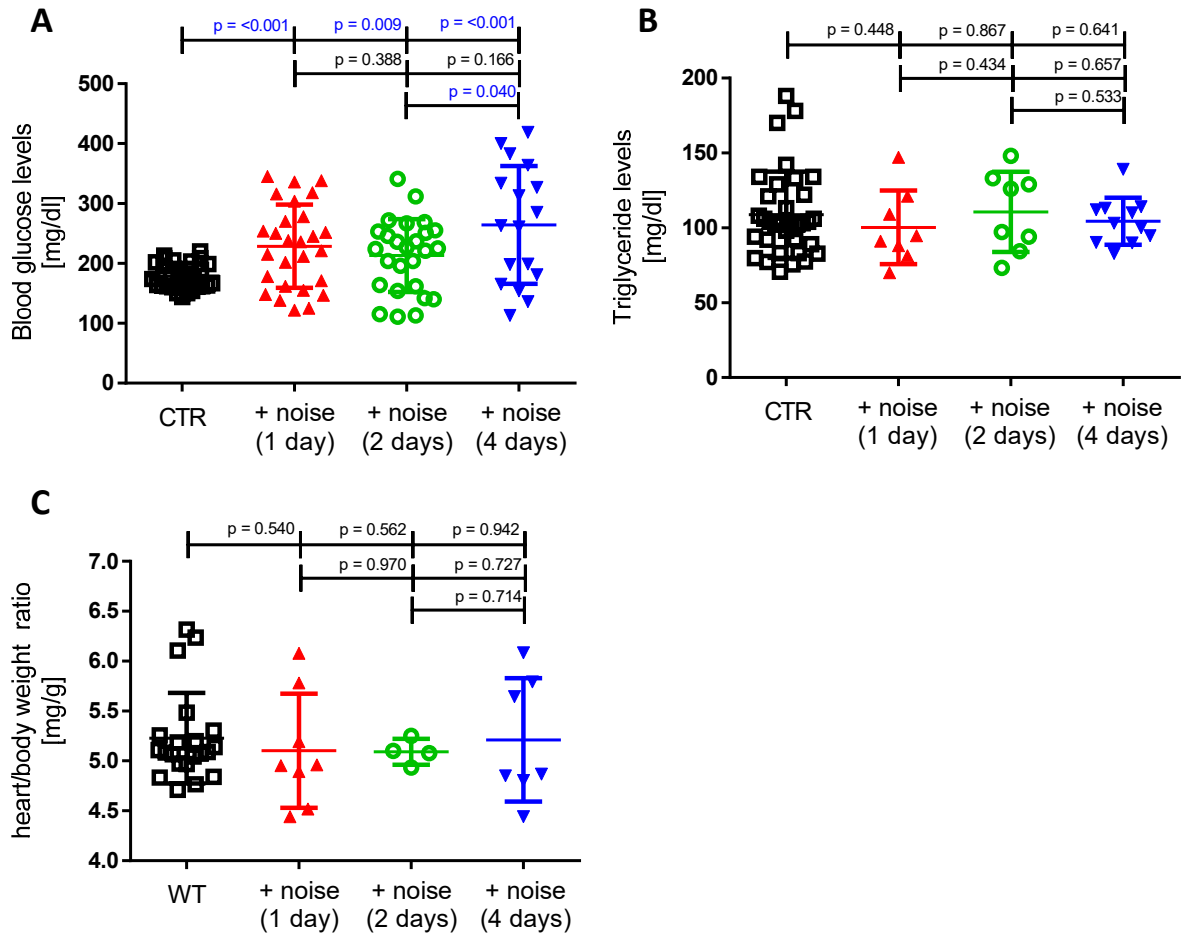

Supplemental Fig. 1S: Effects of noise on blood glucose, triglycerides and Heart/body weight ratio.

(**A**) Noise significantly increased blood glucose levels after 1, 2 and 4 d of exposure. Serum triglyceride levels (**B**) and heart/body weight ratio (**C**) were not changed among the groups. Data are mean ± SD from n = 17-27 (**A**), 8-34 (**B**) and 4-21 (**C**) mice/group.

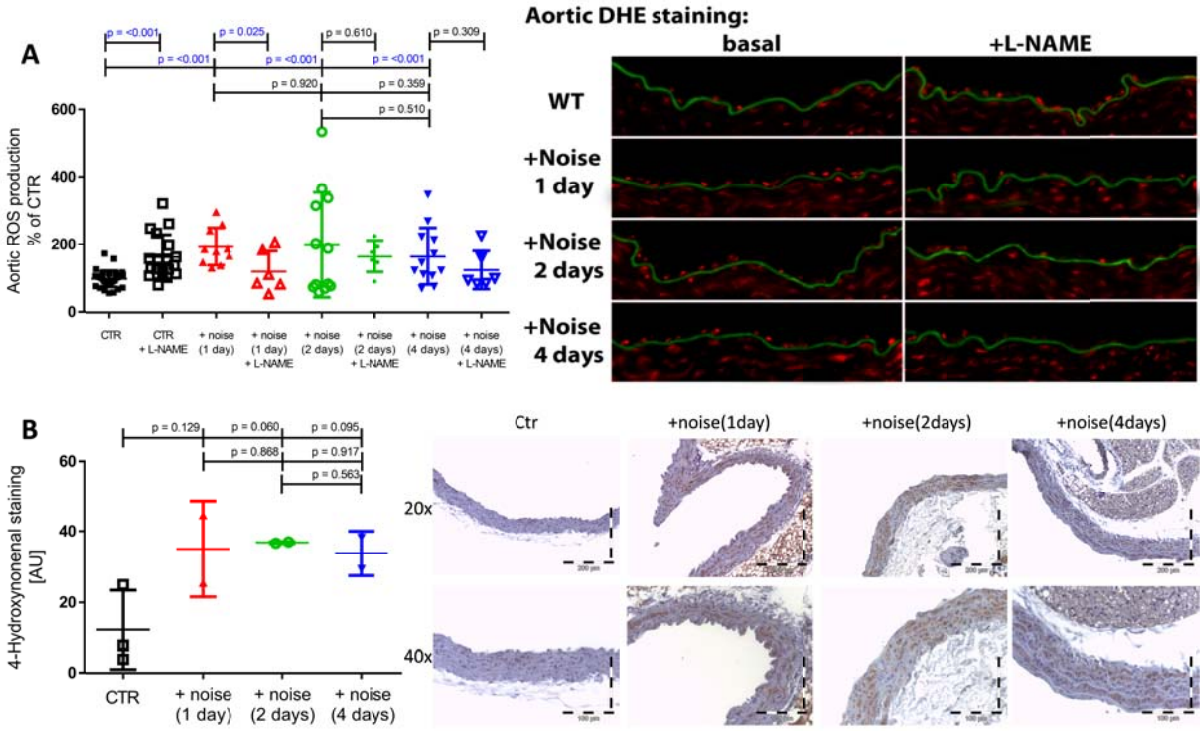

Supplemental Fig. 2S: Effects of noise on superoxide production, eNOS coupling state and lipid peroxidation in aortic tissue.

(**A**) Noise significantly increased ROS signals (dihydroethidium (DHE) fluorescence microtopography) in aortic tissue after 1, 2 and 4 d of exposure. Incubation of aortic rings from mice exposed to noise with L-NAME reduced the ROS signal in the endothelial cell layer providing further evidence for an uncoupled eNOS. Representative DHE stainings are shown beside the quantification. n = 10-35 mice/group (w/o L-NAME) and n = 6-18 mice/group (with L-NAME). (**B**) Noise markedly increased immunostaining of 4-hydroxynonenal-positive proteins of intact aortic rings (brown color). The densitometric analysis revealed an increase by trend in all noise-exposed groups. Representative stainings are shown beside the quantification. Data are mean ± SD from n = 2-3 mice/group.

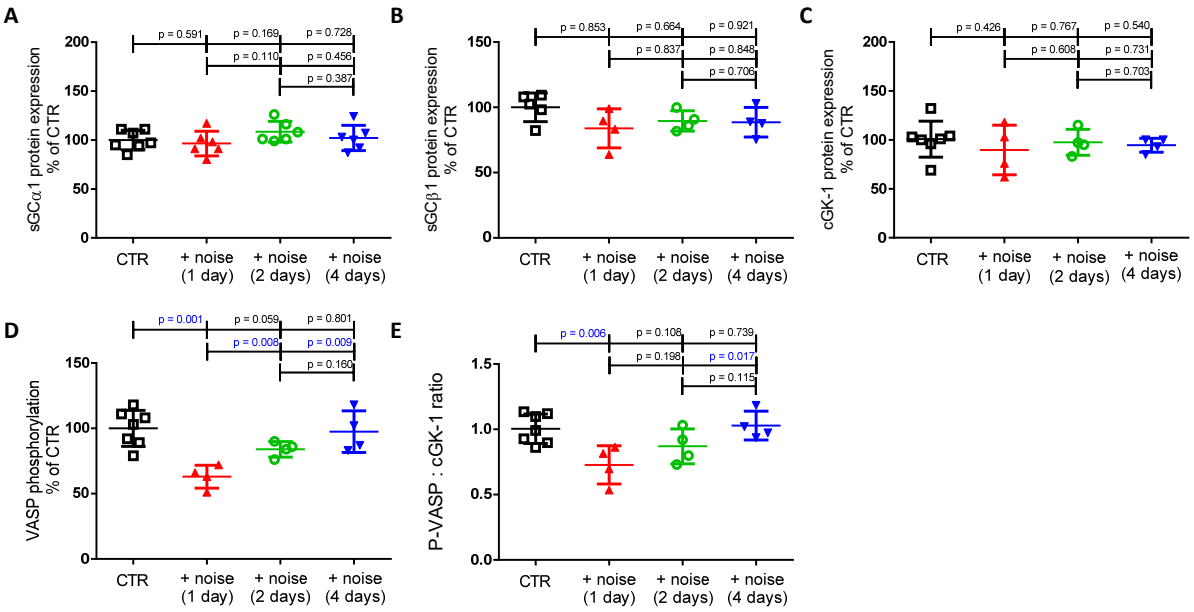

Supplemental Fig. 3S: Effects of noise on vascular NO signaling pathways.

(**A–C**) Aortic protein expression of soluble guanylate cyclase (sGC) and cGMP-dependent protein kinase-1 (cGK-I) was not changed. The activity of cGK-I analyzed by the phosphorylation of the vasodilator stimulated phosphoprotein (VASP, at serine 239) (**D**) and the ratio of p-VASP/cGK-I (**E**) revealed a significant decrease after 1 day of noise exposure. Data are mean ± SD from n=4-7 samples/group (pooled from 2-3 mice per sample) (**A-E**).

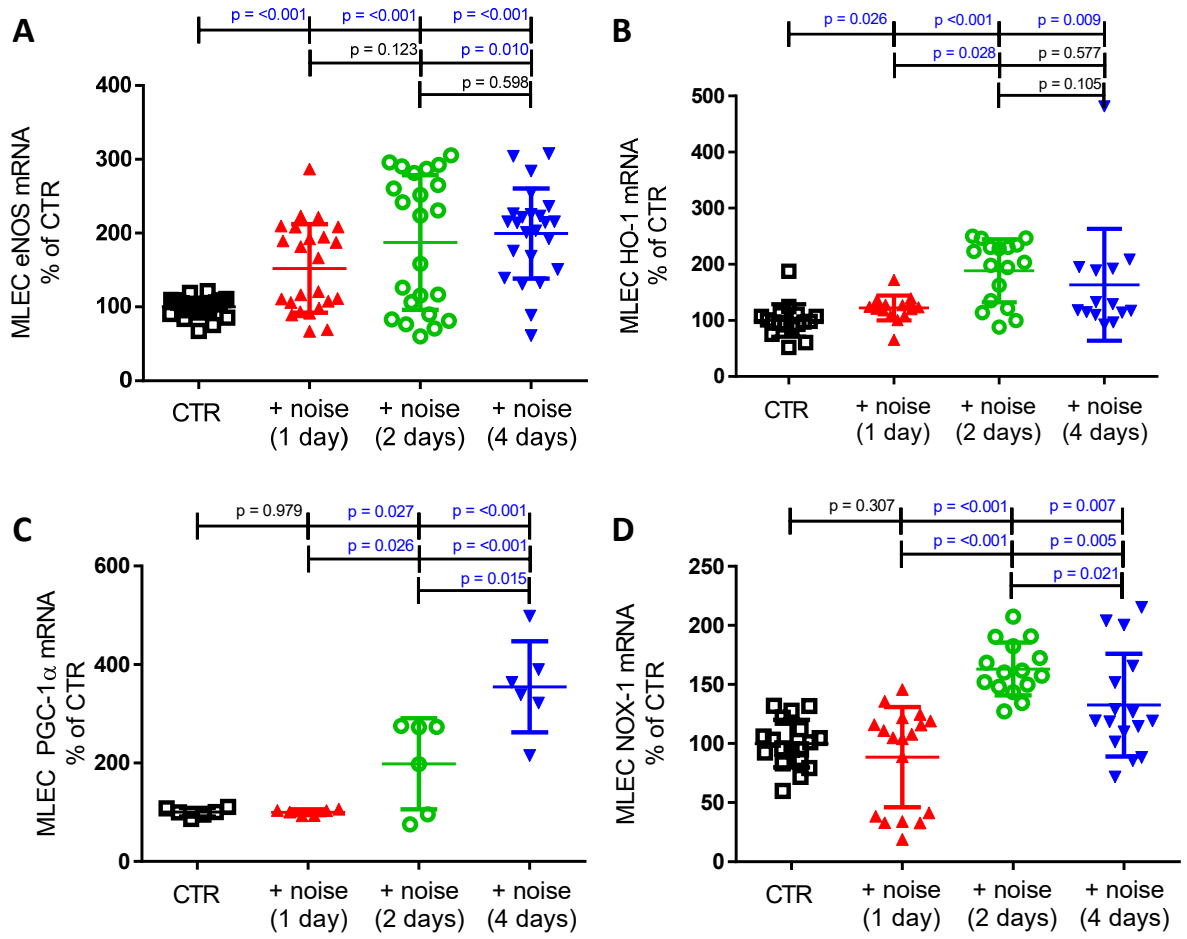

Supplemental Fig. 4S: Endothelial cell specific mRNA expression in murine lung endothelial cells (MLEC) from noise exposed animals.

Endothelial NO synthase was up-regulated significantly in MLEC in response to noise (**A**). Proteins regulating the oxidative stress response like the heme oxygenase-1 (HO-1) (**B**) and PGC-1α (**C**) were up-regulated after 2 and 4 days of noise exposure (HO-1 also after 1 day). NOX-1 expression (isoform of NADPH oxidase) was increased by 2 and 4 days of noise exposure (**D**). Data are mean ± SD from n = 23-24 (**A**), 13-17 (**B**), 6 (**C**) and 15-18 (**D**) mice / group.

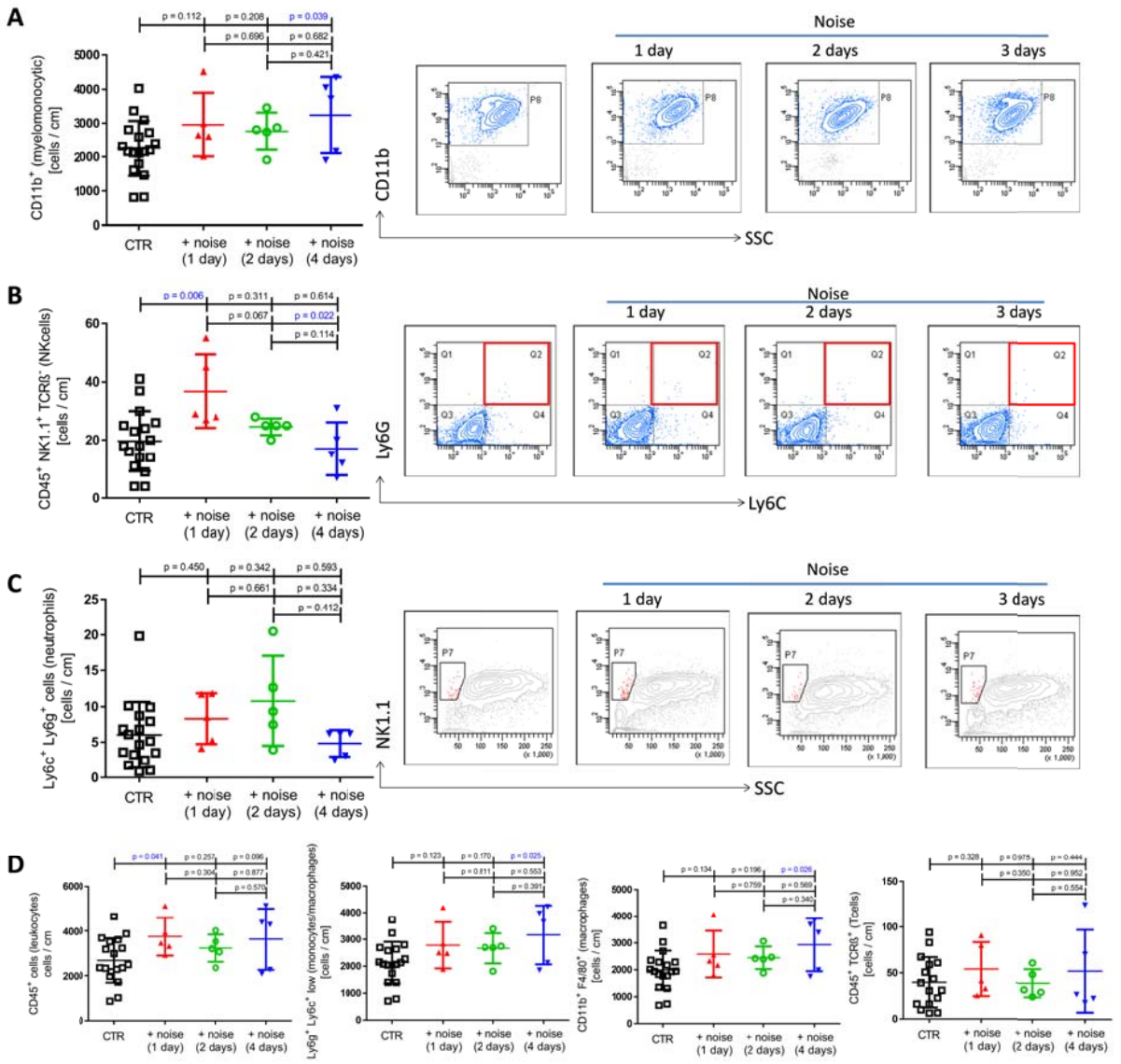

Supplemental Fig. 5S: Effects of noise on infiltration of mouse aorta by inflammatory cells.

Infiltration of total myelomonocytic ($CD11b^+$) cells (**A**) and natural killer ($CD45^+$ $NK1.1^+$ $TCR\beta^-$) cells (**B**) was increased. No significant effect was observed on neutrophils ($Ly6c^+$ $Ly6g^+$ cells) (**C**). Significant increase for at least one of the noise exposure days was observed for leukocytes ($CD45^+$ cells), macrophages/monocytes ($Ly6c^+$low $Ly6g^+$ cells) and macrophages ($CD11b^+$ $F4/80^+$ cells), whereas no change was visible for T cells ($CD45^+$ $TCR\beta^+$ cells) (**D**). Increased infiltration was demonstrated by the FACS blot and single cell counts. Original FACS plots are shown for selected examples beside the quantifications. Data are mean ± SD from n=16-18 (Ctr) and 5 (noise groups) mice/group.

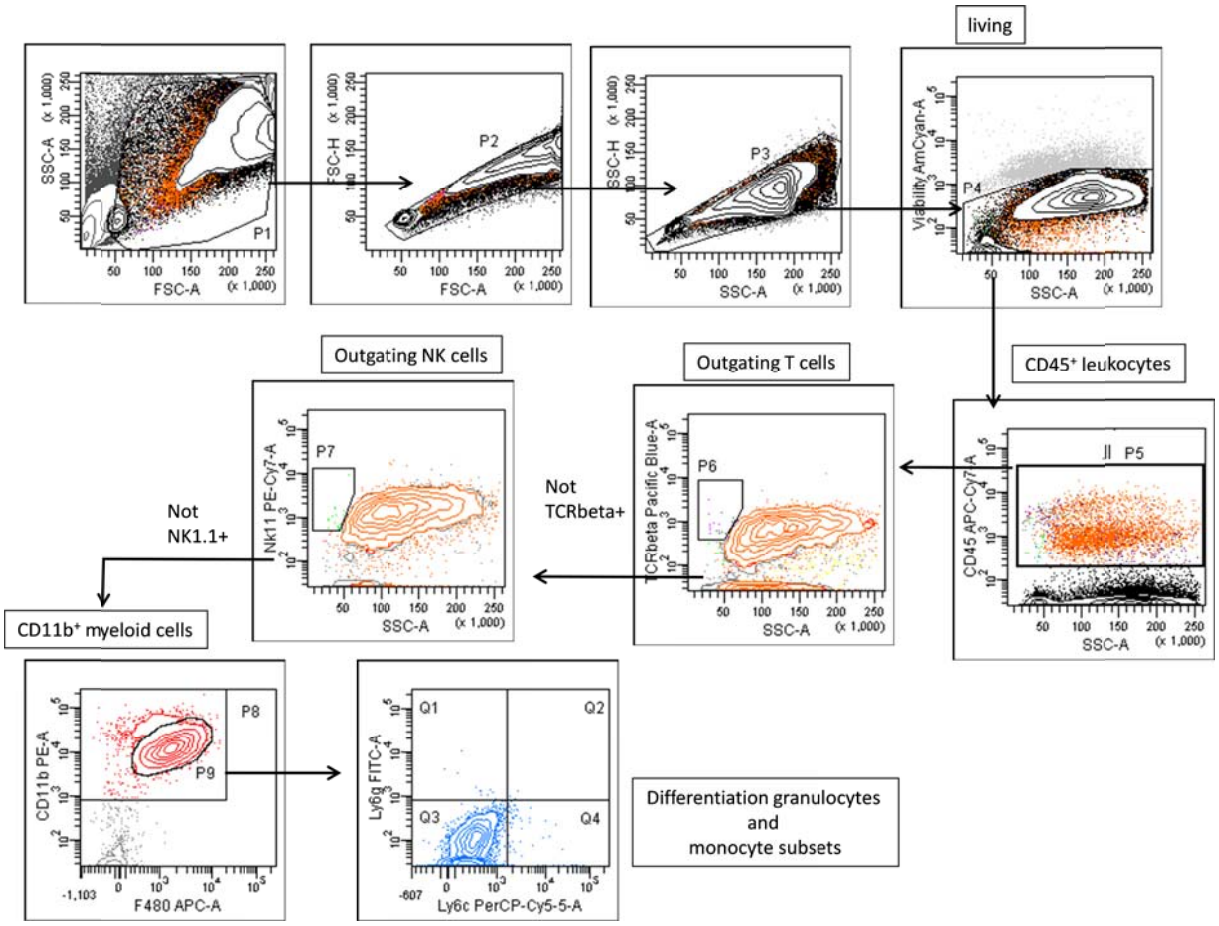

Supplemental Fig. 6S: Gating strategy for FACS analysis.

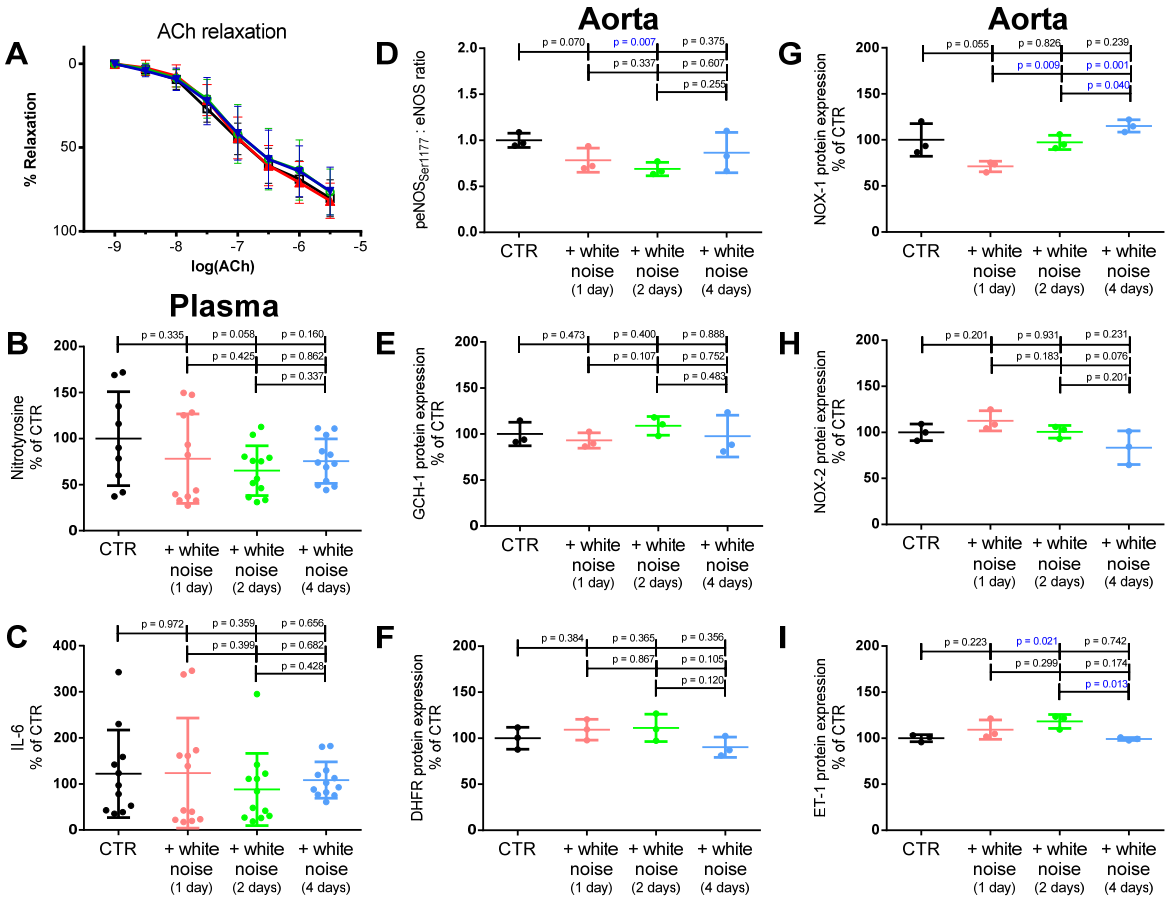

Supplemental Fig. 7S: Effects of white noise for 1, 2 and 4d on endothelial function, NO/cGMP signaling and oxidative stress parameters.

(**A**) Relaxation by the endothelium-dependent vasodilator acetylcholine (ACh) was not changed by white noise exposure (n = 12 mice/group). (**B-C**) Nitrotyrosine-positive proteins and IL-6 levels were not increased in mouse plasma upon white noise exposure. (**D-F**) Endothelial NO synthase phosphorylation at Ser1177, GTP-cyclohydrolase I (GCH-I) and dihydrofolate reductase (DHFR) expression showed no major changes in response to white noise (only one day of noise exposure with significant decrease in eNOS phosphorylation). (**G-H**) Aortic NADPH oxidase subunits NOX-1 and NOX-2 showed no major changes as compared to the control group after white noise exposure. (**I**) Aortic endothelin-1 expression showed no major changes after white noise exposure (only one day of noise exposure with significant increase in ET-1 protein). Data are mean ± SD from n=12 (**A**), 9-12 (**B-C**) mice/group and n = 3 samples (pooled from 3-4 mice per sample) (**D-I**).

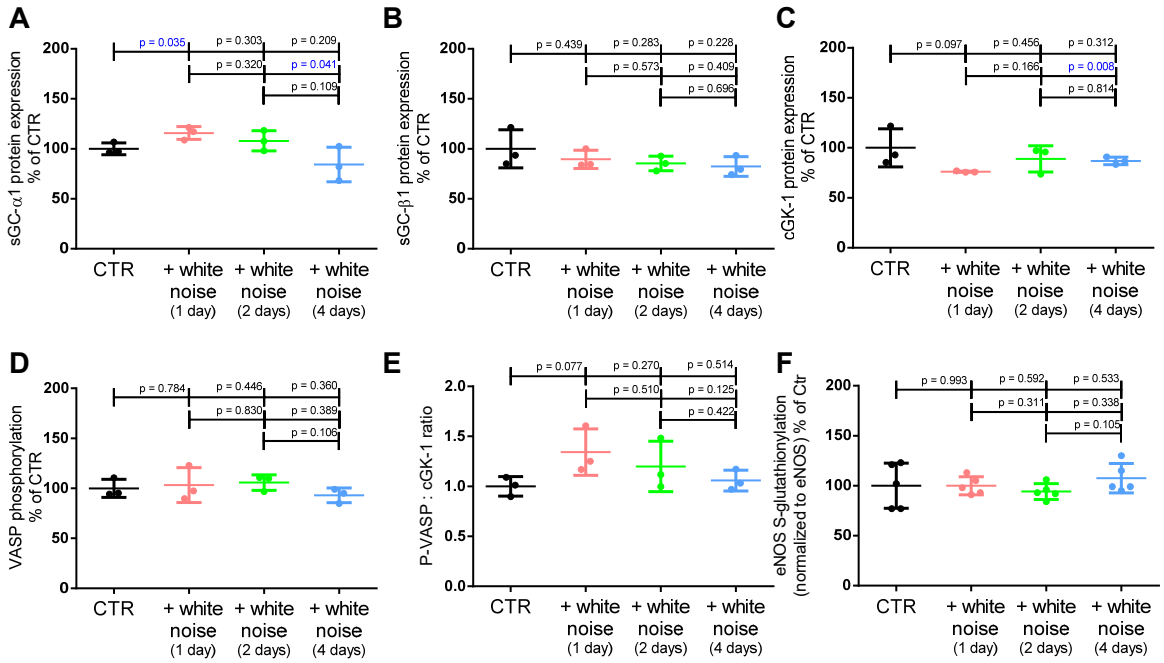

Supplemental Fig. 8S: Effects of white noise on vascular NO signaling pathways.

(**A-C**) Aortic protein expression of soluble guanylate cyclase (sGC) and cGMP-dependent protein kinase-1 (cGK-I) showed no major changes in response to white noise as compared to the control group (only one day of noise exposure with significant increase in sGCalpha). The activity of cGK-I analyzed by the phosphorylation of the vasodilator stimulated phosphoprotein (P-VASP, at serine 239) was not changed in any group (**D**). The ratio of P-VASP/cGK-I (**E**) increased by trend after 1 day of white noise exposure. Cardiac S-glutathionylation of eNOS, the marker for eNOS uncoupling, was not changed in any group (**F**). Data are mean ± SD from n = 3 samples (pooled from 3-4 mice per sample) (**A-E**) and 5 samples (pooled from 2-3 mice per sample) (**F**).

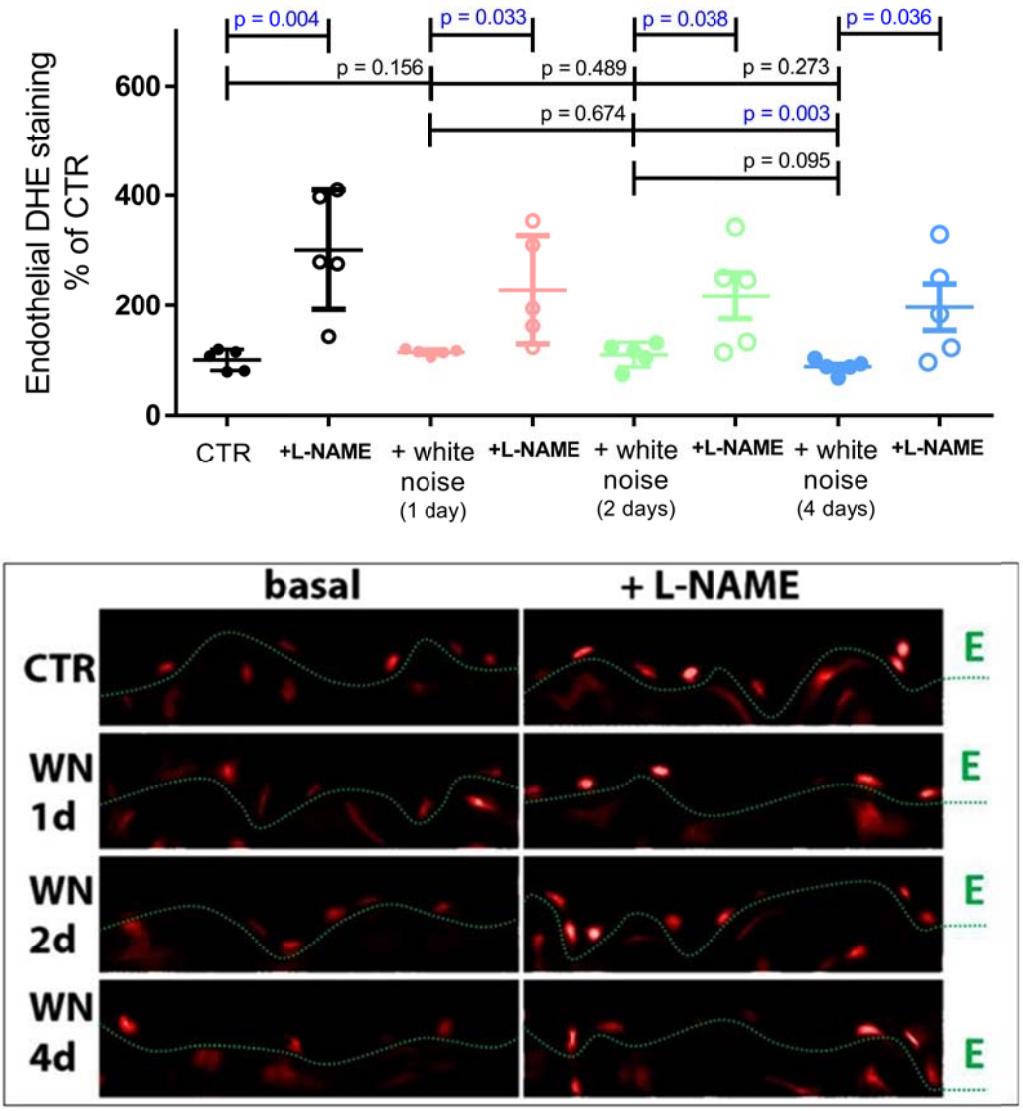

Supplemental Fig. 9S: Effects of white noise on superoxide production and eNOS coupling state.

White noise did not increase ROS signals (dihydroethidium (DHE) fluorescence microtopography) in the endothelial cell layer of aortic ring segments after 1, 2 and 4 d of exposure. Incubation of aortic rings from mice exposed to white noise with L-NAME increased the ROS signal in the endothelial cell layer providing further evidence for a coupled eNOS. Representative DHE stainings are shown below the quantification. Data are mean ± SD from n = 5 mice/group.

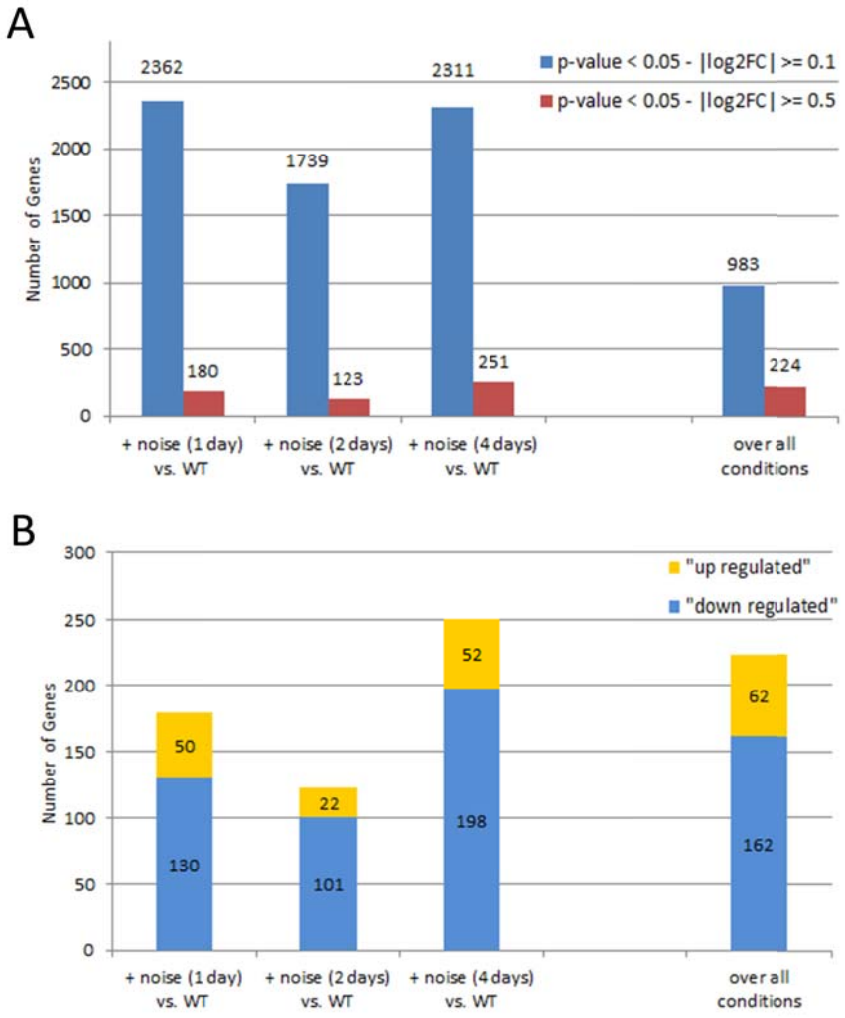

Supplemental Fig. 10S: Effects of noise (4d) on gene expression in mouse aorta.

(A) DESeq2 analysis of the sequence data identifies 2362 (1 day noise exposure) significantly down- or up-regulated genes (p-value > 0.05) if compared to untreated controls. (B). If a threshold of |log2FC| > 0.5 is chosen, there are still between 123 (1 day) and 251 (4 days) genes significantly up or down regulated

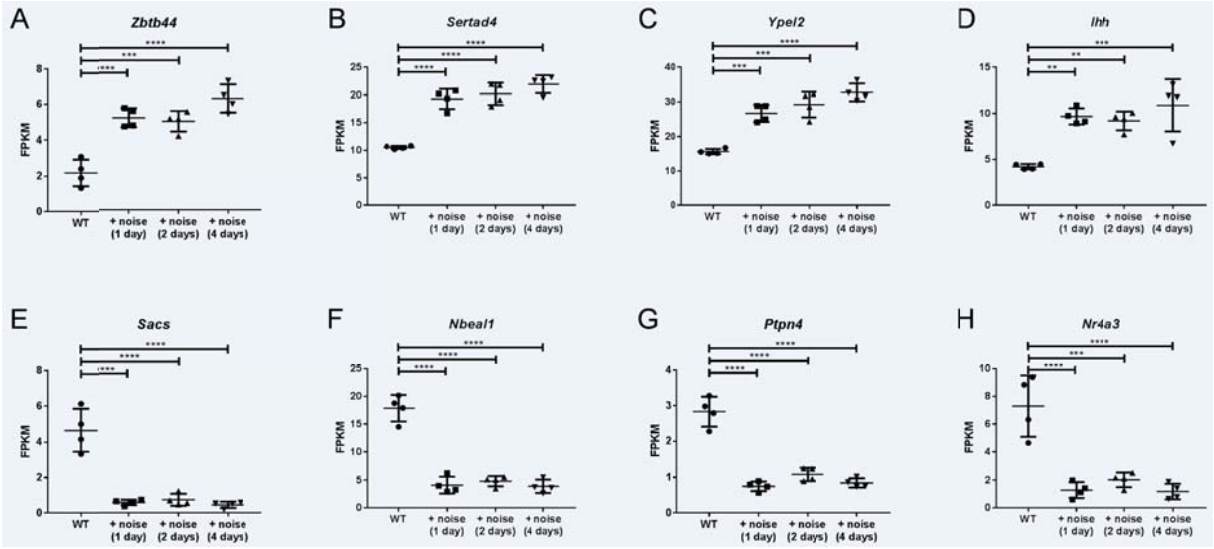

Supplemental Fig. 11S: Strongest up- and down regulated genes

The whisker plots show the four strongest up (A-D) and down regulated genes (E-H) in mouse aorta after one, two of four days of noise exposure compared to no noise. Data are mean ± SD from n = 4/group, * p<0.05, ** p<=0.002, *** p<=0.0002, **** p<0.0001.

A Supplemental Fig. **12S**

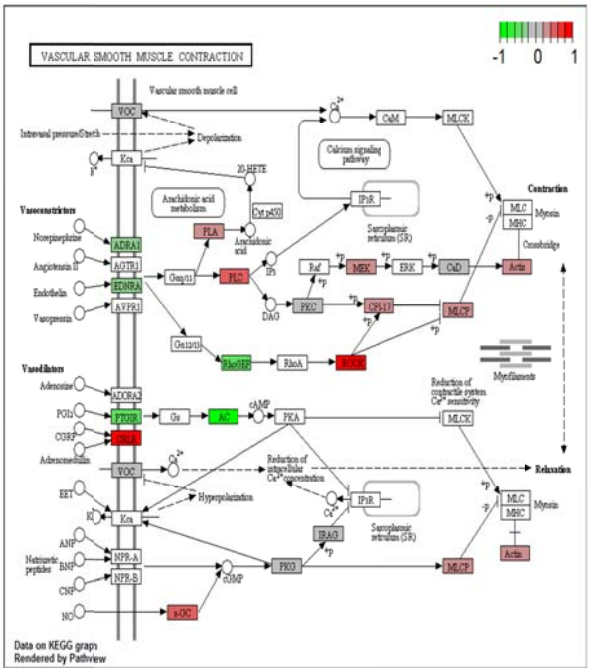

B

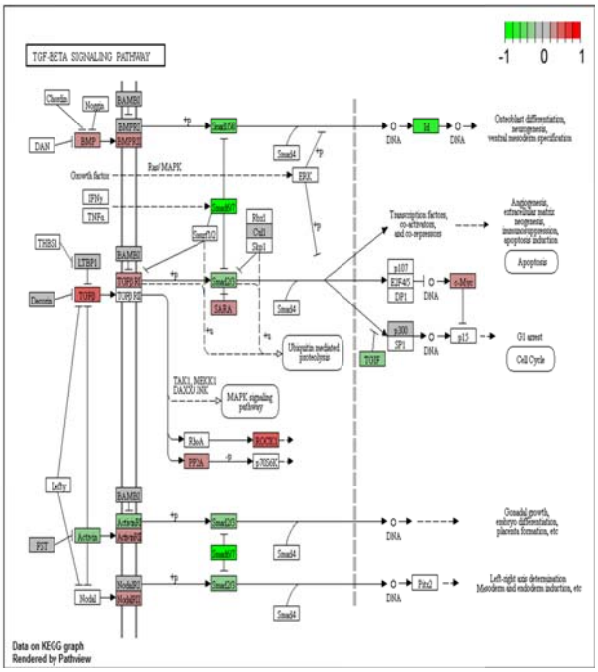

A Supplemental Fig. **13S**

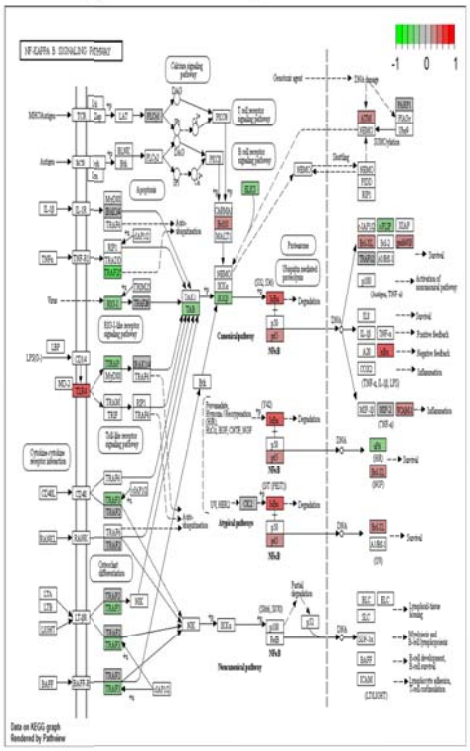

B

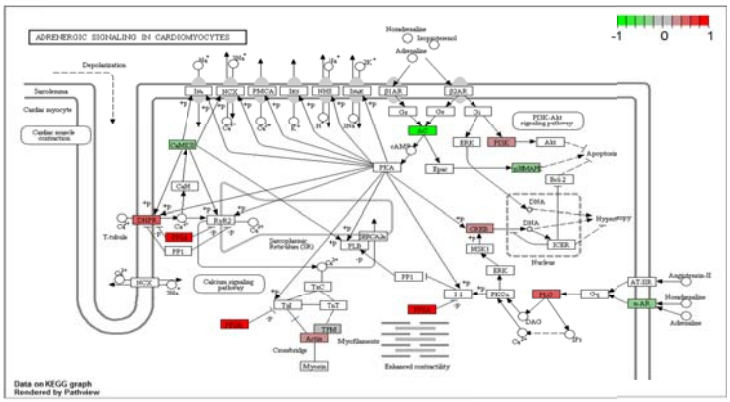

C

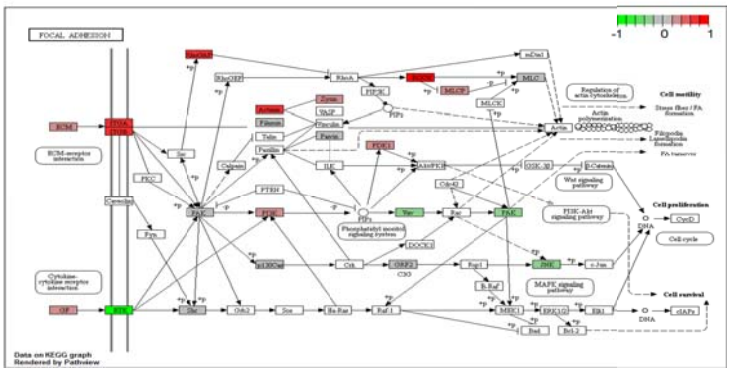

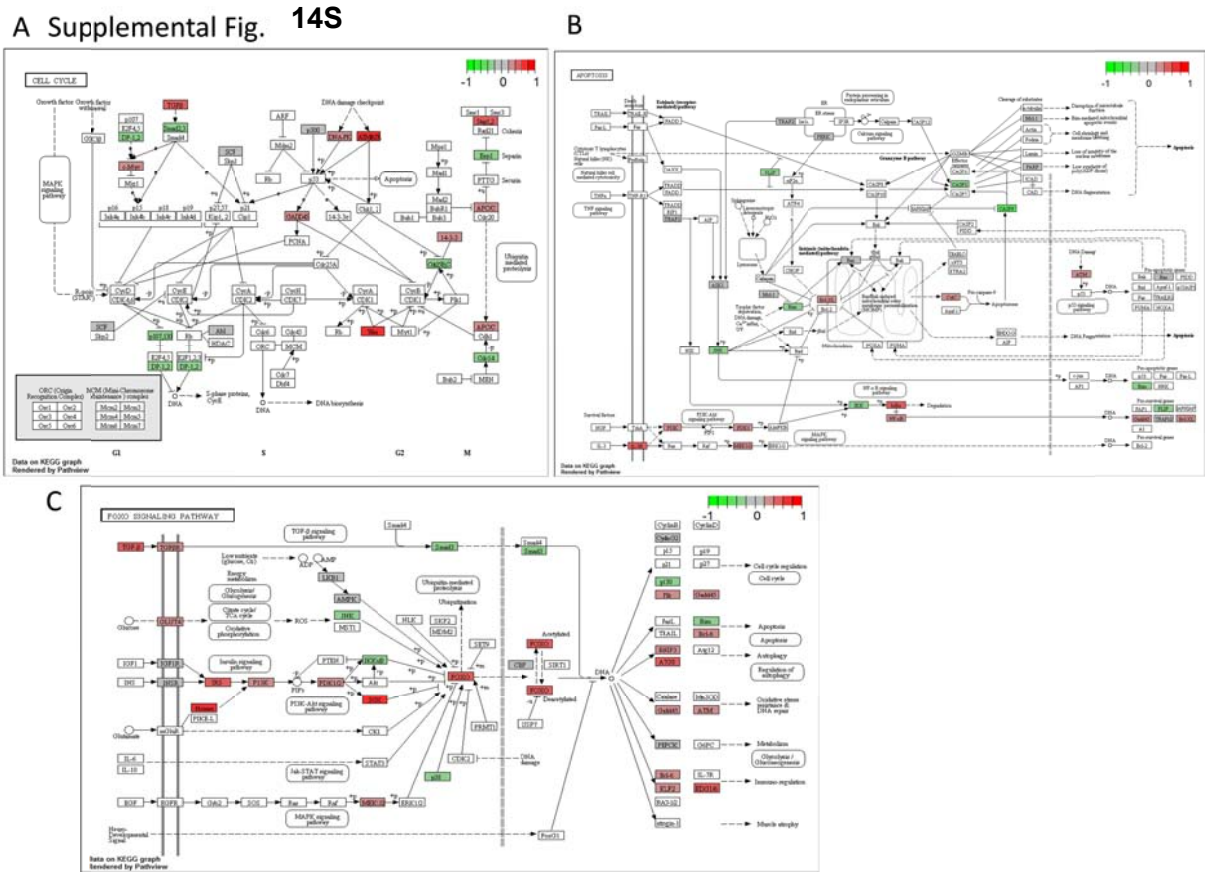

Supplemental Fig. 12-14S: Gene expression changes in selected pathways.

Visualization based on mean expression changes demonstrate that cluster of genes in specific pathways are hit predominantly when they are known to be involved in the same pathway. Noise exposure for only one day led to significant changes in the expression of genes involved in the regulation of mechanisms affecting cell and vascular structure as well as cell survival. Color scaled log2 fold changes shows genes expressed higher (green) and lower (red) in treated groups than in controls relative to the highest lowest (1/-1) value ($p < 0.05$).

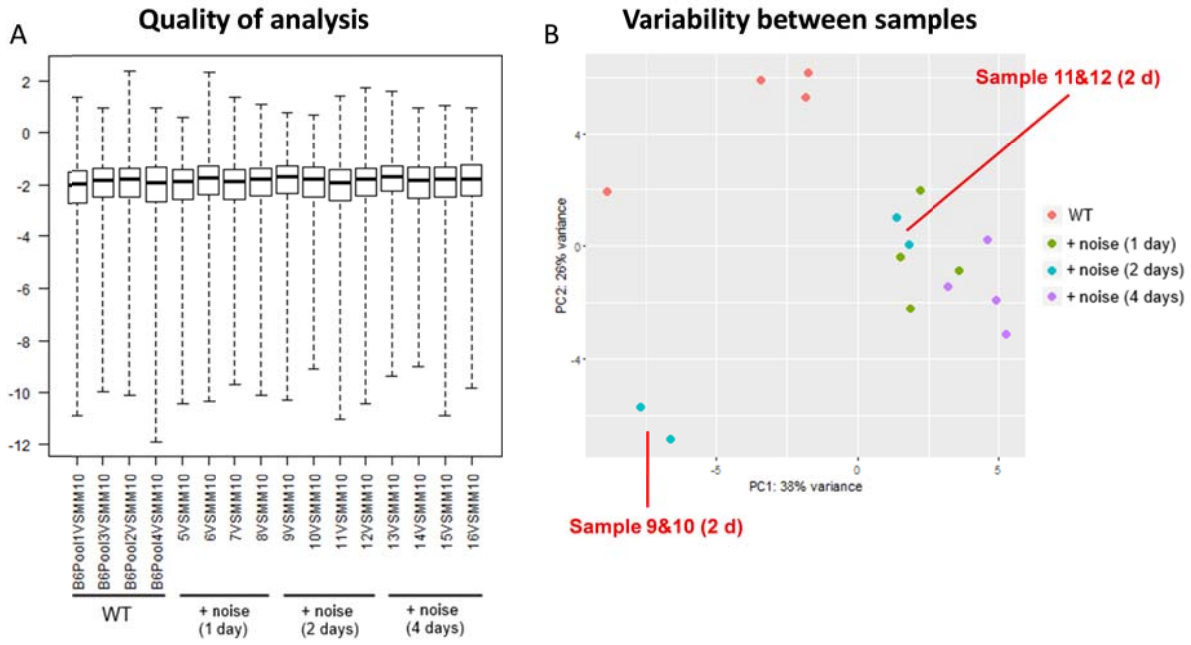

Supplemental Fig. 15S: Outlier detection in RNA-Seq data.

(A) Boxplot of Cook's distances (DESeq2) shows homogeneous low distances among all samples. (B) In the principle component analysis (PCA – DSeq2) the samples mainly cluster according to the experimental groups. Only one (out of 4) of the control pool data sets and two (out of 4 of day 2 noise groups) show deviant ("outlying") expression values.

Supplemental Fig. **16S**

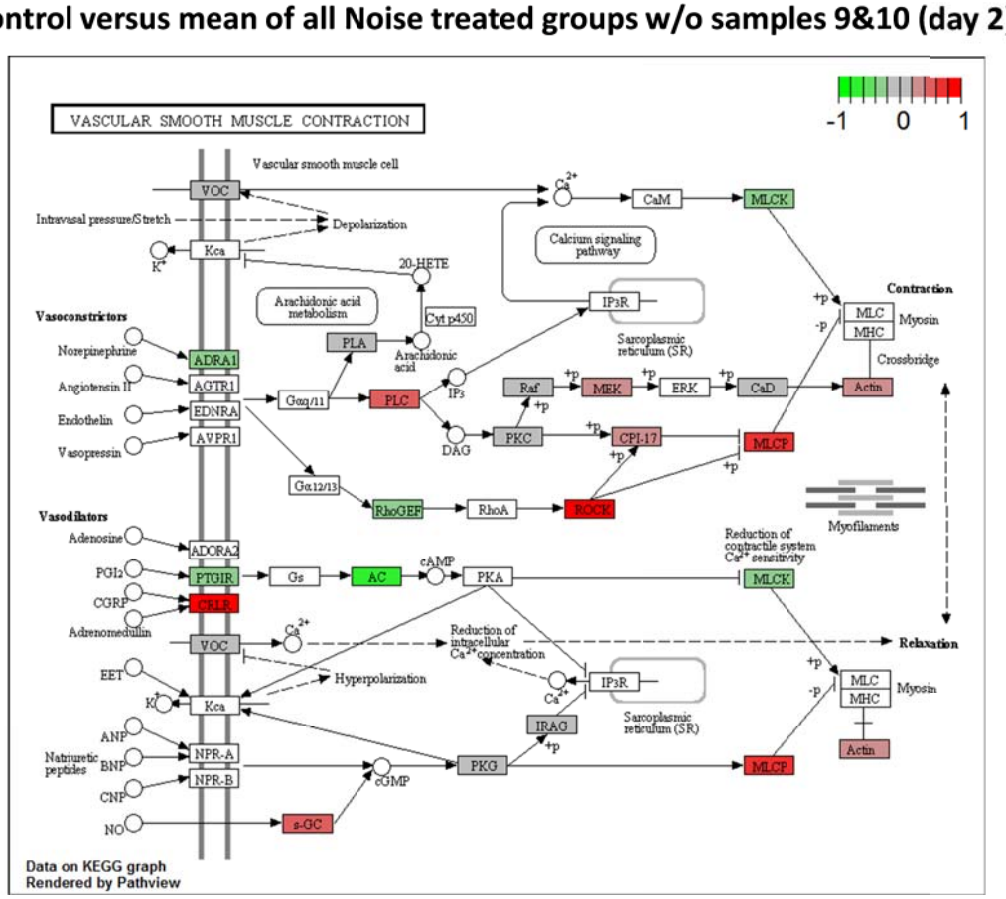

Supplemental Fig. 16S: Gene expression changes in vascular smooth muscle contraction pathway.

Same as suppl. Fig. 12S, panel A but with outlier samples 9&10 (see suppl. Fig. 15S) excluded for calculation.

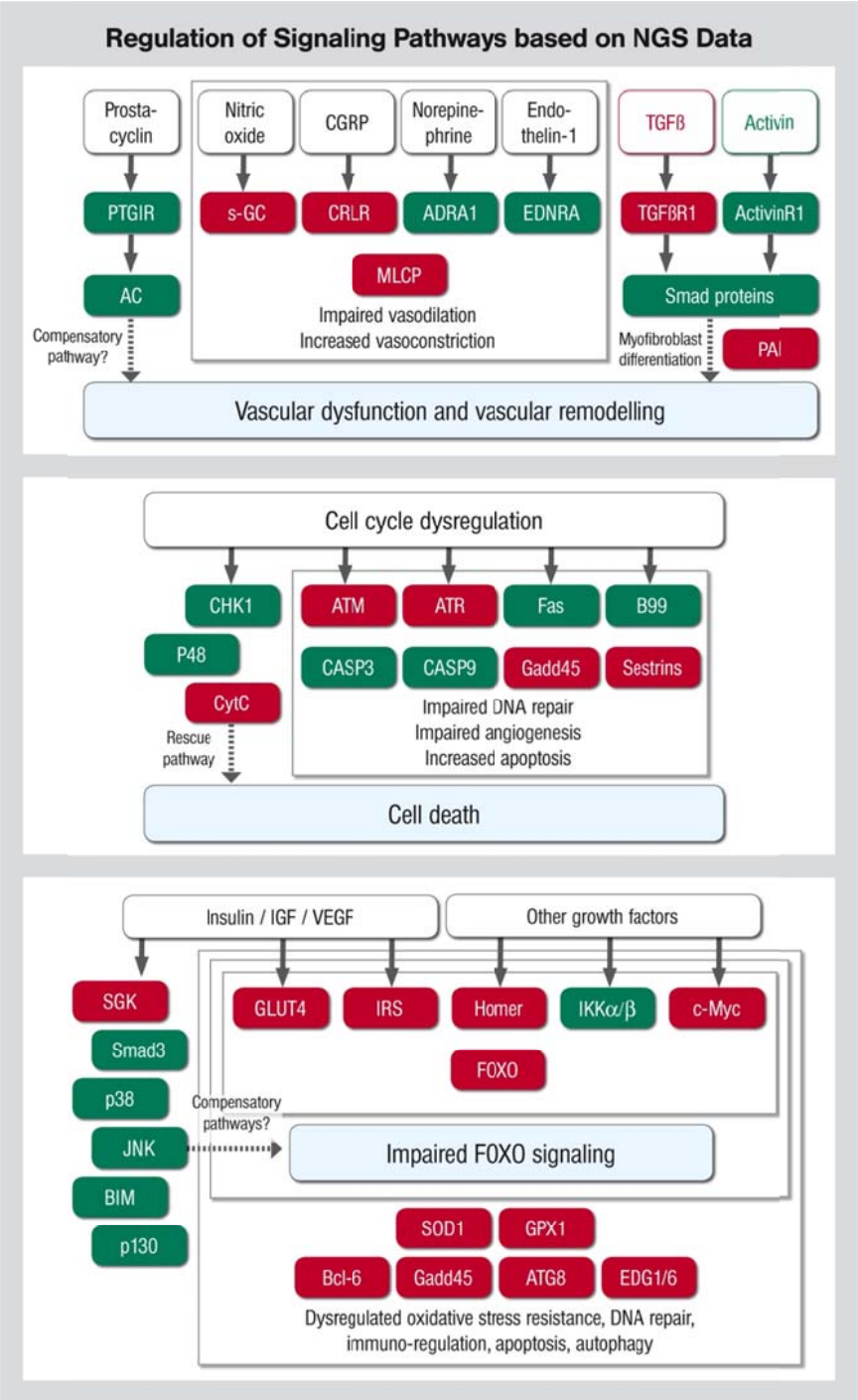

Supplemental Fig. 17S: Summary scheme of most relevant signalling pathways as the result of the next generation sequencing (NGS) experiments. Upregulated genes are in green, downregulated genes are red solid boxes. PTGIR, prostaglandin I2 receptor; AC, adenylyl cyclase; s-GC, soluble guanylyl cyclase; CGRP, calcitonin gene-related peptide; CRLR, calcitonin receptor-like receptor; ADRA1, adrenergic receptor alpha 1; EDNRA, endothelin receptor type A; TGFβ, transforming growth factor beta; TGFβR1, transforming growth factor beta-receptor 1; Smad, group of intracellular proteins that act down-stream to extracellular TGFβ signals; PAI, plasminogen activator inhibitor; CHK1, checkpoint kinase 1; P48/PTF1, DNA binding

protein involved in transcription and DNA repair; CytC, cytochrome c; ATM, Ataxia telangiectasia mutated is an important checkpoint kinase; ATR, Ataxia telangiectasia and Rad3 related is a protein kinase; Fas, CD95 (cluster of differentiation 95); B99, G2 And S-Phase Expressed 1, gene involved in cell cycle; CASP3/9, caspase-3/-9; Gadd45, growth arrest and DNA damage-inducible 45 proteins; SGK, serum- and glucocorticoid-induced protein kinase; p38, mitogen-activated protein (MAP) kinase; JNK, c-Jun N-terminal kinase; BIM, Bcl-2 interacting mediator of cell death; p130, RBL2, regulator of entry into cell division; IGF, insulin-like growth factor; VEGF, vascular endothelial growth factor; GLUT4, glucose transporter type 4; IRS, insulin receptor substrate; Homer, homer scaffolding proteins; IKKα/β, inhibitor of nuclear factor kappa-B kinase α/β; c-Myc, nuclear phosphoprotein that plays a role in cell cycle progression and apoptosis; FOXO, Forkhead box proteins O is a group of transcription factors involved in cell growth, proliferation and differentiation; SOD1, intracellular Cu,Zn-superoxide dismutase; GPX-1, glutathione peroxidase-1; Bcl-6, B-cell lymphoma 6 protein; ATG8, autophagy-related protein 8; EDG1/6, endothelial differentiation gene 1/6 or sphingosine-1-phosphate receptor 1/6.

Supplemental References

1. Munzel T, Giaid A, Kurz S, Stewart DJ, Harrison DG. Evidence for a role of endothelin 1 and protein kinase C in nitroglycerin tolerance. Proc Natl Acad Sci 1995;**92**(11):5244-8.
2. Oelze M, Knorr M, Kroller-Schon S, Kossmann S, Gottschlich A, Rummler R, Schuff A, Daub S, Doppler C, Kleinert H, Gori T, Daiber A, Munzel T. Chronic therapy with isosorbide-5-mononitrate causes endothelial dysfunction, oxidative stress, and a marked increase in vascular endothelin-1 expression. Eur Heart J 2013;**34**(41):3206-16.
3. Mollnau H, Oelze M, Zinssius E, Hausding M, Wu Z, Knorr M, Ghaemi Kerahrodi J, Kroller-Schon S, Jansen T, Teutsch C, Foster C, Li H, Wenzel P, Schulz E, Munzel T, Daiber A. Effects of telmisartan or amlodipine monotherapy versus telmisartan/amlodipine combination therapy on vascular dysfunction and oxidative stress in diabetic rats. Naunyn-Schmiedeberg's archives of pharmacology 2013;**386**(5):405-19.
4. Oelze M, Kroller-Schon S, Welschof P, Jansen T, Hausding M, Mikhed Y, Stamm P, Mader M, Zinssius E, Agdauletova S, Gottschlich A, Steven S, Schulz E, Bottari SP, Mayoux E, Munzel T, Daiber A. The sodium-glucose co-transporter 2 inhibitor empagliflozin improves diabetes-induced vascular dysfunction in the streptozotocin diabetes rat model by interfering with oxidative stress and glucotoxicity. PLoS One 2014;**9**(11):e112394.
5. Oelze M, Daiber A, Brandes RP, Hortmann M, Wenzel P, Hink U, Schulz E, Mollnau H, von Sandersleben A, Kleschyov AL, Mulsch A, Li H, Forstermann U, Munzel T. Nebivolol inhibits superoxide formation by NADPH oxidase and endothelial dysfunction in angiotensin II-treated rats. Hypertension 2006;**48**(4):677-84.
6. Wenzel P, Schulz E, Oelze M, Muller J, Schuhmacher S, Alhamdani MS, Debrezion J, Hortmann M, Reifenberg K, Fleming I, Munzel T, Daiber A. AT1-receptor blockade by telmisartan upregulates GTP-cyclohydrolase I and protects eNOS in diabetic rats. Free Radic Biol Med 2008;**45**(5):619-26.
7. Oelze M, Knorr M, Schuhmacher S, Heeren T, Otto C, Schulz E, Reifenberg K, Wenzel P, Munzel T, Daiber A. Vascular dysfunction in streptozotocin-induced experimental diabetes strictly depends on insulin deficiency. J Vasc Res 2011;**48**(4):275-84.
8. Schuhmacher S, Oelze M, Bollmann F, Kleinert H, Otto C, Heeren T, Steven S, Hausding M, Knorr M, Pautz A, Reifenberg K, Schulz E, Gori T, Wenzel P, Munzel T, Daiber A. Vascular dysfunction in experimental diabetes is improved by pentaerithrityl tetranitrate but not isosorbide-5-mononitrate therapy. Diabetes 2011;**60**(10):2608-16.
9. Kroller-Schon S, Steven S, Kossmann S, Scholz A, Daub S, Oelze M, Xia N, Hausding M, Mikhed Y, Zinssius E, Mader M, Stamm P, Treiber N, Scharffetter-Kochanek K, Li H, Schulz E, Wenzel P, Munzel T, Daiber A. Molecular mechanisms of the crosstalk between mitochondria and NADPH oxidase through reactive oxygen species-studies in white blood cells and in animal models. Antioxid Redox Signal 2014;**20**(2):247-66.
10. Kleschyov AL, Munzel T. Advanced spin trapping of vascular nitric oxide using colloid iron diethyldithiocarbamate. Methods Enzymol 2002;**359**:42-51.
11. Feng M, Whitesall S, Zhang Y, Beibel M, D'Alecy L, DiPetrillo K. Validation of volume-pressure recording tail-cuff blood pressure measurements. Am J Hypertens 2008;**21**(12):1288-91.
12. Wenzel P, Knorr M, Kossmann S, Stratmann J, Hausding M, Schuhmacher S, Karbach SH, Schwenk M, Yogev N, Schulz E, Oelze M, Grabbe S, Jonuleit H, Becker C, Daiber A, Waisman A, Munzel T. Lysozyme M-positive monocytes mediate angiotensin II-induced arterial hypertension and vascular dysfunction. Circulation 2011;**124**:1370-1381.
13. Kossmann S, Schwenk M, Hausding M, Karbach SH, Schmidgen MI, Brandt M, Knorr M, Hu H, Kroller-Schon S, Schonfelder T, Grabbe S, Oelze M, Daiber A, Munzel T,

Becker C, Wenzel P. Angiotensin II-induced vascular dysfunction depends on interferon-gamma-driven immune cell recruitment and mutual activation of monocytes and NK-cells. Arterioscler Thromb Vasc Biol 2013;**33**(6):1313-9.
14. Dobin A, Davis CA, Schlesinger F, Drenkow J, Zaleski C, Jha S, Batut P, Chaisson M, Gingeras TR. STAR: ultrafast universal RNA-seq aligner. Bioinformatics 2013;**29**(1):15-21.
15. Li B, Dewey CN. RSEM: accurate transcript quantification from RNA-Seq data with or without a reference genome. BMC bioinformatics 2011;**12**:323.
16. Team RC. R: A Language and Environment for Statistical Computing. Vienna, Austria 2016.
17. Love MI, Huber W, Anders S. Moderated estimation of fold change and dispersion for RNA-seq data with DESeq2. Genome biology 2014;**15**(12):550.
18. Ogata H, Goto S, Sato K, Fujibuchi W, Bono H, Kanehisa M. KEGG: Kyoto Encyclopedia of Genes and Genomes. Nucleic acids research 1999;**27**(1):29-34.
19. Kanehisa M, Sato Y, Kawashima M, Furumichi M, Tanabe M. KEGG as a reference resource for gene and protein annotation. Nucleic acids research 2016;**44**(D1):D457-62.
20. Luo W, Brouwer C. Pathview: an R/Bioconductor package for pathway-based data integration and visualization. Bioinformatics 2013;**29**(14):1830-1.
21. Schmidt F, Kolle K, Kreuder K, Schnorbus B, Wild P, Hechtner M, Binder H, Gori T, Munzel T. Nighttime aircraft noise impairs endothelial function and increases blood pressure in patients with or at high risk for coronary artery disease. Clin Res Cardiol 2015;**104**(1):23-30.
22. Faul F, Erdfelder E, Lang AG, Buchner A. G*Power 3: a flexible statistical power analysis program for the social, behavioral, and biomedical sciences. Behav Res Methods 2007;**39**(2):175-91.
23. Wistow G, Bernstein SL, Ray S, Wyatt MK, Behal A, Touchman JW, Bouffard G, Smith D, Peterson K. Expressed sequence tag analysis of adult human iris for the NEIBank Project: steroid-response factors and similarities with retinal pigment epithelium. Molecular vision 2002;**8**:185-95.
24. Brandenberger R, Wei H, Zhang S, Lei S, Murage J, Fisk GJ, Li Y, Xu C, Fang R, Guegler K, Rao MS, Mandalam R, Lebkowski J, Stanton LW. Transcriptome characterization elucidates signaling networks that control human ES cell growth and differentiation. Nature biotechnology 2004;**22**(6):707-16.
25. Pilot-Storck F, Chopin E, Rual JF, Baudot A, Dobrokhotov P, Robinson-Rechavi M, Brun C, Cusick ME, Hill DE, Schaeffer L, Vidal M, Goillot E. Interactome mapping of the phosphatidylinositol 3-kinase-mammalian target of rapamycin pathway identifies deformed epidermal autoregulatory factor-1 as a new glycogen synthase kinase-3 interactor. Molecular & cellular proteomics : MCP 2010;**9**(7):1578-93.
26. Glatter T, Wepf A, Aebersold R, Gstaiger M. An integrated workflow for charting the human interaction proteome: insights into the PP2A system. Molecular systems biology 2009;**5**:237.
27. Arking DE, Pulit SL, Crotti L, van der Harst P, Munroe PB, Koopmann TT, Sotoodehnia N, Rossin EJ, Morley M, Wang X, Johnson AD, Lundby A, Gudbjartsson DF, Noseworthy PA, Eijgelsheim M, Bradford Y, Tarasov KV, Dorr M, Muller-Nurasyid M, Lahtinen AM, Nolte IM, Smith AV, Bis JC, Isaacs A, Newhouse SJ, Evans DS, Post WS, Waggott D, Lyytikainen LP, Hicks AA, Eisele L, Ellinghaus D, Hayward C, Navarro P, Ulivi S, Tanaka T, Tester DJ, Chatel S, Gustafsson S, Kumari M, Morris RW, Naluai AT, Padmanabhan S, Kluttig A, Strohmer B, Panayiotou AG, Torres M, Knoflach M, Hubacek JA, Slowikowski K, Raychaudhuri S, Kumar RD, Harris TB, Launer LJ, Shuldiner AR, Alonso A, Bader JS, Ehret G, Huang H, Kao WH, Strait JB, Macfarlane PW, Brown M, Caulfield MJ, Samani NJ, Kronenberg F, Willeit J, Smith JG, Greiser KH, Meyer Zu Schwabedissen H, Werdan K, Carella M, Zelante L, Heckbert SR, Psaty BM, Rotter JI,

Kolcic I, Polasek O, Wright AF, Griffin M, Daly MJ, Arnar DO, Holm H, Thorsteinsdottir U, Denny JC, Roden DM, Zuvich RL, Emilsson V, Plump AS, Larson MG, O'Donnell CJ, Yin X, Bobbo M, D'Adamo AP, Iorio A, Sinagra G, Carracedo A, Cummings SR, Nalls MA, Jula A, Kontula KK, Marjamaa A, Oikarinen L, Perola M, Porthan K, Erbel R, Hoffmann P, Jockel KH, Kalsch H, Nothen MM, den Hoed M, Loos RJ, Thelle DS, Gieger C, Meitinger T, Perz S, Peters A, Prucha H, Sinner MF, Waldenberger M, de Boer RA, Franke L, van der Vleuten PA, Beckmann BM, Martens E, Bardai A, Hofman N, Wilde AA, Behr ER, Dalageorgou C, Giudicessi JR, Medeiros-Domingo A, Barc J, Kyndt F, Probst V, Ghidoni A, Insolia R, Hamilton RM, Scherer SW, Brandimarto J, Margulies K, Moravec CE, del Greco MF, Fuchsberger C, O'Connell JR, Lee WK, Watt GC, Campbell H, Wild SH, El Mokhtari NE, Frey N, Asselbergs FW, Mateo Leach I, Navis G, van den Berg MP, van Veldhuisen DJ, Kellis M, Krijthe BP, Franco OH, Hofman A, Kors JA, Uitterlinden AG, Witteman JC, Kedenko L, Lamina C, Oostra BA, Abecasis GR, Lakatta EG, Mulas A, Orru M, Schlessinger D, Uda M, Markus MR, Volker U, Snieder H, Spector TD, Arnlov J, Lind L, Sundstrom J, Syvanen AC, Kivimaki M, Kahonen M, Mononen N, Raitakari OT, Viikari JS, Adamkova V, Kiechl S, Brion M, Nicolaides AN, Paulweber B, Haerting J, Dominiczak AF, Nyberg F, Whincup PH, Hingorani AD, Schott JJ, Bezzina CR, Ingelsson E, Ferrucci L, Gasparini P, Wilson JF, Rudan I, Franke A, Muhleisen TW, Pramstaller PP, Lehtimaki TJ, Paterson AD, Parsa A, Liu Y, van Duijn CM, Siscovick DS, Gudnason V, Jamshidi Y, Salomaa V, Felix SB, Sanna S, Ritchie MD, Stricker BH, Stefansson K, Boyer LA, Cappola TP, Olsen JV, Lage K, Schwartz PJ, Kaab S, Chakravarti A, Ackerman MJ, Pfeufer A, de Bakker PI, Newton-Cheh C. Genetic association study of QT interval highlights role for calcium signaling pathways in myocardial repolarization. Nature genetics 2014;**46**(8):826-36.

28. Wang S, Yang K, Chen S, Wang J, Du G, Fan S, Wei L. Indian hedgehog contributes to human cartilage endplate degeneration. European spine journal : official publication of the European Spine Society, the European Spinal Deformity Society, and the European Section of the Cervical Spine Research Society 2015;**24**(8):1720-8.

29. Handorf AM, Chamberlain CS, Li WJ. Endogenously produced Indian Hedgehog regulates TGFbeta-driven chondrogenesis of human bone marrow stromal/stem cells. Stem Cells Dev 2015;**24**(8):995-1007.

30. Sun Y, Daemen A, Hatzivassiliou G, Arnott D, Wilson C, Zhuang G, Gao M, Liu P, Boudreau A, Johnson L, Settleman J. Metabolic and transcriptional profiling reveals pyruvate dehydrogenase kinase 4 as a mediator of epithelial-mesenchymal transition and drug resistance in tumor cells. Cancer & Metabolism 2014;**2**.

31. Chen J, Lu Y, Xu J, Huang Y, Cheng H, Hu G, Luo C, Lou M, Cao G, Xie Y, Ying K. Identification and characterization of NBEAL1, a novel human neurobeachin-like 1 protein gene from fetal brain, which is up regulated in glioma. Brain research Molecular brain research 2004;**125**(1-2):147-55.

32. Zhou J, Wan B, Shan J, Shi H, Li Y, Huo K. PTPN4 negatively regulates CrkI in human cell lines. Cellular & molecular biology letters 2013;**18**(2):297-314.

33. Rodriguez-Calvo R, Ferran B, Alonso J, Marti-Pamies I, Aguilo S, Calvayrac O, Rodriguez C, Martinez-Gonzalez J. NR4A receptors up-regulate the antiproteinase alpha-2 macroglobulin (A2M) and modulate MMP-2 and MMP-9 in vascular smooth muscle cells. Thromb Haemost 2015;**113**(6):1323-34.

34. Rodríguez-Calvo R, Guadall A, Calvayrac O, Navarro MA, Alonso J, Ferrán B, de Diego A, Muniesa P, Osada J, Rodríguez C, Martínez-González J. Over-expression of Neuron-derived Orphan Receptor-1 (NOR-1) exacerbates neointimal hyperplasia after vascular injury. Human molecular genetics 2013;**22**(10):1949-1959.

35. Forte A, Della Corte A, De Feo M, Cerasuolo F, Cipollaro M. Role of myofibroblasts in vascular remodelling: focus on restenosis and aneurysm. Cardiovasc Res 2010;**88**(3):395-405.